Mon. Not. R. Astron. Soc. **343,** 585–607 (2003)

Starburst and AGN activity in ultraluminous infrared galaxies

D. Farrah,[1⋆] J. Afonso,[2,3] A. Efstathiou,[4] M. Rowan-Robinson,[5] M. Fox[5] and D. Clements[5]

[1]*SIRTF Science Centre, California Institute of Technology, Jet Propulsion Laboratory, Pasadena, CA 91125, USA*
[2]*CAAUL, Observatório Astronómico de Lisboa, Tapada da Ajuda, 1349-018 Lisboa, Portugal*
[3]*Onsala Space Observatory, S-43992 Onsala, Sweden*
[4]*Department of Computer Science and Engineering, Cyprus College, 6 Diogenous Street, PO Box 22006, 1516 Nicosia, Cyprus*
[5]*Astrophysics Group, Blackett Laboratory, Imperial College, Prince Consort Road, London SW7 2BW*

Accepted 2003 April 7. Received 2003 April 7; in original form 2002 December 13

ABSTRACT

We examine the power source of 41 local ultraluminous infrared galaxies (ULIRGs) using archival infrared (IR) and optical photometry. We fit the observed spectral energy distributions with starburst and active galactic nucleus (AGN) components, each component being drawn from a family of templates. We find that all of the sample require a starburst, whereas only half require an AGN. In 90 per cent of the sample the starburst provides over half the IR emission, with a mean fractional luminosity of 82 per cent. When combined with other galaxy samples we find that starburst and AGN luminosities correlate over six decades in IR luminosity, suggesting that a common factor governs both luminosities, plausibly the gas masses in the nuclear regions. We find no trend for increasing fractional AGN luminosity with increasing total luminosity, contrary to previous claims. We find that the mid-IR $F_{7.7}/C_{7.7}$ line-continuum ratio is no indication of the starburst luminosity, or the fractional AGN luminosity, and therefore that $F_{7.7}/C_{7.7}$ is not a reliable diagnostic of the power source in ULIRGs. The radio flux correlates with the starburst luminosity, but shows no correlation with the AGN luminosity, in line with previous results. We propose that the scatter in this correlation is due to a skewed starburst initial mass function and/or relic relativistic electrons from a previous starburst, rather than contamination from an obscured AGN. We show that most ULIRGs undergo multiple starbursts during their lifetime, and by inference that mergers between more than two galaxies may be common amongst ULIRGs. Our results support the evolutionary model for ULIRGs proposed by Farrah et al., where they can follow many different evolutionary paths of starburst and AGN activity in transforming merging spiral galaxies into elliptical galaxies, but that most do not go through an optical quasi-stellar object phase. The lower level of AGN activity in our local sample compared with $z \sim 1$ hyperluminous infrared galaxies implies that the two samples are distinct populations. We postulate that different galaxy formation processes at high z are responsible for this difference.

Key words: galaxies: active – quasars: general – galaxies: Seyfert – galaxies: starburst – infrared: galaxies.

1 INTRODUCTION

One of the most important results from the *Infrared Astronomical Satellite* (*IRAS*) all-sky surveys was the detection of a new class of galaxy where most of the bolometric emission lies in the infrared waveband (Soifer et al. 1984; Sanders & Mirabel 1996). These 'luminous infrared galaxies' (LIRGs), become the dominant extragalactic population at infrared (IR) luminosities above 10^{11} $L_{\odot}$, with a higher space density than all other classes of galaxy of comparable bolometric luminosity. At the most luminous end of the *IRAS* galaxy population lie the ultraluminous infrared galaxies (ULIRGs), those with $L_{\rm ir} > 10^{12}$ $L_{\odot}$. Although ULIRGs are rare in the local Universe, their luminosity function shows strong evolution with redshift (Veilleux, Sanders & Kim 1999) and deep submillimetre surveys (Barger et al. 1998; Hughes

⋆E-mail: duncan@ipac.caltech.edu

et al. 1998; Eales et al. 2000; Fox et al. 2002; Scott et al. 2002) have found that systems with ULIRG-like luminosities are very numerous at $z \geqslant 1$. ULIRGs are thus an important population in understanding the cosmic history of star formation. ULIRGs are also thought to play a role in the evolution of spiral and elliptical galaxies. Nearly all ULIRGs are observed to be ongoing mergers between two or more spirals (Sanders et al. 1988; Farrah et al. 2001), and it is thought that such a merger will form an elliptical (Barnes 1989).

Despite this, the evolution of ULIRGs, their power source and the trigger behind the IR emission are poorly understood. Although it is now accepted that a mixture of star formation and active galactic nucleus (AGN) activity powers the IR emission, the *dominant* power source, and how ULIRGs evolve, are unknown. There are similarities between ULIRGs and starburst galaxies (Joseph & Wright 1985; Rowan-Robinson & Crawford 1989; Condon et al. 1991). Conversely, many ULIRGs display emission lines characteristic of Seyferts (Sanders et al. 1988). An early evolutionary model for ULIRGs was that of Sanders et al. (1988) who suggested, based on the similar space density, bolometric emission and luminosity function of ULIRGs and quasi-stellar objects (QSOs) in the local Universe, that ULIRGs are the dust enshrouded precursors to optical QSOs and that all QSOs emerge from a luminous infrared phase. Conversely, a more recent evolutionary model (Farrah et al. 2001) proposes that ULIRGs are not a simple dust-shrouded precursor to optical QSOs but instead follow multiple evolutionary paths.

In this paper we examine the power source in ULIRGs, their evolution, and their relationship to high-z IR luminous galaxies using archival photometry for a sample of 41 local ULIRGs, and advanced radiative transfer models for starbursts and AGN. We also examine the origin of the radio–IR correlation in ULIRGs and the power of mid-IR spectroscopy as a diagnostic of the active power source. Sample selection and data analysis are described in Sections 2 and 3. Results are presented in Section 4 and notes on individual objects are given in Section 5. A discussion is presented in Section 6 and conclusions are summarized in Section 7. We adopt $H_0 = 65$ km s^{-1} Mpc^{-1}, $\Omega_0 = 1.0$ and $\Lambda = 0.0$ and quote all luminosities in this system. Unless otherwise stated, the terms 'IR luminosity', 'starburst luminosity' and 'AGN luminosity' refer to the luminosity over the wavelength range 1–1000 μm. Luminosities are quoted in units of bolometric solar luminosities, where $L_\odot = 3.826 \times 10^{26}$ W.

2 THE SAMPLE

We assembled from the literature a sample of objects comprising all ULIRGs with $z \leqslant 0.1$. This was complicated by the fact that different authors use different minimum luminosities for ULIRGs (e.g. Condon et al. 1991, $L_{40-120} \geqslant 10^{11.02}$ $L_\odot$; Clements et al. 1996, $L_{60} \geqslant 10^{11.77}$ $L_\odot$). We first adopted our own minimum IR luminosity for a ULIRG, namely a rest-frame 1–1000 μm luminosity (hereafter referred to as $L_{\rm ir}$) of greater than 10^{12} $L_\odot$. Using a luminosity derived across a broad wavelength range is to be preferred, as luminosities derived across smaller wavelength ranges may erroneously exclude or include objects due to their continuum shape. We then assembled a parent sample of all objects claimed to be ULIRGs, or close to ULIRG luminosity, at $z \leqslant 0.1$, from the *IRAS* Point Source Catalogue, the *IRAS* Faint Source Catalogue, and the sample presented by Clements et al. (1996). We then determined their 1–1000 μm luminosities using the methods described in Sections 3 and 4, and excluded those objects that did not satisfy our luminosity criterion. From a parent sample of 73 objects, 32 were excluded. The final sample of 41 objects, presented in Table 1, are all contained within the *IRAS* Point Source Catalogue. This final sample thus comprises a complete sample of ULIRGs at $z < 0.1$ with $L_{\rm ir} > 10^{12}$ $L_\odot$, and is thus free from selection effects arising from infrared colours, or luminosities measured across smaller-wavelength ranges.

Fluxes were assembled from on-line catalogues and from the literature. Optical and near-IR fluxes were taken from the APM and 2MASS data bases and also from Carico et al. (1988) and Spinoglio et al. (1995). *IRAS* fluxes were taken from the *IRAS* Faint Source Survey. The XSCANPI software was used to derive *IRAS* fluxes where only upper limits were present in the catalogues. Other infrared data were taken from Carico et al. (1988), Maiolino et al. (1995), Klaas et al. (1997), Rigopoulou et al. (1999), Dale et al. (2000), Zink et al. (2000), Klaas et al. (2001) and Tran et al. (2001). Submillimetre data were taken from Rigopoulou, Lawrence & Rowan-Robinson (1996), Dunne et al. (2000) and Dunne & Eales (2001). The assembled optical and near-infrared photometry is listed in Table 2. The assembled infrared and submillimetre photometry is listed in Table 3.

3 INFRARED EMISSION MODELS

3.1 Starburst models

To model the IR emission due to starburst activity we used the starburst models of Efstathiou, Rowan-Robinson & Siebenmorgen (2000). These models consider an ensemble of evolving H II regions containing hot young stars, embedded within giant molecular clouds (GMCs) of gas and dust. The composition of the dust is given by the dust grain model of Siebenmorgen & Kruegel (1992), which includes the polycyclic aromatic hydrocarbons (PAHs) thought to be responsible for the 7.7-μm emission feature. The stellar populations within the GMCs evolve according to the stellar synthesis codes of Bruzual & Charlot (1993). The star formation rate is assumed to decay exponentially with an e-folding time-scale of 2×10^7 yr. The models vary in starburst age from zero years up to 7.2×10^7 yr (11 discrete values) and in effective visual optical depth from $\tau_V = 50$ to 200 (four discrete values). A plot showing the range in starburst spectral energy distribution (SED) template shapes can be found in fig. 3 of Efstathiou et al. (2000), with additional information in fig. 1 of the same paper.

3.2 AGN torus models

To model the IR emission due to AGN, we used the AGN models of Efstathiou & Rowan-Robinson (1995). These models incorporate accurate solutions to the axially symmetric radiative-transfer problem in dust clouds to model the IR emission from dust in active galactic nuclei. Dust composition is given by the multigrain dust model of Rowan-Robinson (1992). We have used the thick tapered disc models following an r^{-1} density distribution, as this subset of models has been found to be most successful in satisfying the observational constraints of AGN. The AGN models vary in torus opening angle from 0° to 90° (15 discrete values) and in ultraviolet (UV) equatorial optical depth, from $\tau_{\rm UV} = 1000$ to 1500 (three discrete values). A plot showing the range in AGN torus SED template shapes can be found in fig. 5 of Efstathiou & Rowan-Robinson (1995).

Table 1. All ultraluminous infrared galaxies at $z < 0.1$.

IRAS name	Other names	RA (2000) (hh:mm:ss)	Dec. (deg arcmin arcsec)	z	Optical spectrum	F_{25}/F_{60}^{a}
00198−7926		00 21 52.9	−79 10 08.0	0.0728	Sy2	0.370
00199−7426		00 22 07.0	−74 09 41.6	0.0964	–	0.078
00262+4251		00 28 54.2	+43 08 15.3	0.0927	LINER	0.112
00335−2732		00 36 00.5	−27 15 34.5	0.0693	Starburst	0.147
01388−4618		01 40 55.9	−46 02 53.3	0.0903	H II	0.121
02364−4751		02 38 13.1	−47 38 10.5	0.0983	–	0.063
03068−5346		03 08 21.3	−53 35 12.0	0.0745	–	0.057
04232+1436		04 26 05.0	+14 43 38.0	0.0796	LINER	0.113
05189−2524		05 21 01.5	−25 21 45.4	0.0426	Sy2	0.252
06035−7102		06 02 54.0	−71 03 10.3	0.0795	H II	0.112
06206−6315		06 21 01.2	−63 17 23.2	0.0924	Sy2	0.074
08572+3915		09 00 25.4	+39 03 54.4	0.0584	LINER	0.229
09111−1007		09 13 38.8	−10 19 20.3	0.0541	H II+Sy2	0.067
09320+6134	UGC 05101	09 35 51.7	+61 21 11.3	0.0394	LINER+Sy2	0.090
09583+4714		10 01 31.2	+46 59 44.0	0.0859	Sy1+Sy2	0.182
10035+4852		10 06 46.1	+48 37 44.1	0.0648	Starburst	0.062
10190+1322		10 21 42.5	+13 06 53.9	0.0766	H II	0.114
10494+4424		10 52 23.6	+44 08 47.3	0.0921	LINER	0.047
10565+2448		10 59 18.1	+24 32 34.3	0.0431	H II+LINER	0.094
12112+0305		12 13 45.7	+02 48 40.3	0.0733	LINER	0.060
12540+5708	Mrk 231	12 56 14.2	+56 52 25.2	0.0422	Sy1	0.271
13428+5608	Mrk 273	13 44 42.1	+55 53 12.6	0.0378	Sy2	0.105
14348−1447		14 37 38.4	−15 00 22.8	0.0827	LINER	0.072
14378−3651		14 40 58.9	−37 04 33.0	0.0676	LINER+Sy2	0.085
15250+3609		15 26 59.4	+35 58 37.5	0.0552	LINER	0.182
15327+2340	Arp220	15 34 57.1	+23 30 11.5	0.0181	LINER	0.076
17132+5313		17 14 20.5	+53 10 30.4	0.0509	H II+AGN	0.109
17208−0014		17 23 21.9	−00 17 00.4	0.0428	H II	0.053
18470+3233		18 48 54.2	+32 37 31.0	0.0784	H II	0.104
19254−7245	Super-Antenna	19 31 21.6	−72 39 21.7	0.0617	Sy2	0.226
19297−0406		19 32 20.7	−04 00 06.0	0.0857	H II	0.084
19458+0944		19 48 15.7	+09 52 05.0	0.0999	–	0.066
20046−0623		20 07 19.4	−06 14 26.0	0.0844	Starburst	0.141
20414−1651		20 44 18.2	−16 40 16.2	0.0871	H II	0.079
20551−4250		20 58 26.9	−42 39 06.2	0.0428	H II	0.149
21130−4446		21 16 18.5	−44 33 37.7	0.0926	H II	0.048
21504−0628		21 53 05.5	−06 14 49.9	0.0776	–	0.111
22491−1808		22 51 49.3	−17 52 23.4	0.0778	H II	0.101
23128−5919		23 15 47.0	−59 03 16.9	0.0446	H II+Sy2	0.147
23365+3604		23 39 01.3	+36 21 08.7	0.0645	H II+LINER	0.114
23389−6139		23 41 43.6	−61 22 50.9	0.0928	H II	0.067

Coordinates, optical spectral classifications and redshifts were taken from the NASA Extragalactic Data base. [a]Ratio of the *IRAS* 25-μm flux to the *IRAS* 60-μm flux.

4 RESULTS

4.1 Spectral energy distributions

We combined the archival photometry from the optical to the millimetre to fit spectral energy distributions for each object. The goodness of fit was examined using the reduced χ^2 statistic. Fits for all sources were good, with $\chi^2_{\rm best} \leqslant 5$ in all cases and $\chi^2_{\rm best} \leqslant 4$ in all but one case (this object, IRAS 17208-0014, is discussed further in Section 5). To determine the errors on the model parameters we explored reduced χ^2 space between $\chi^2_{\rm best}$ and $\chi^2_{\rm best} + 2$. The resulting luminosities, model parameters and errors are given in Table 4. The SEDs are presented in Fig. 1.

Emission from unobscured population II stars from the merger progenitors is not included in either the starburst or AGN models, and care must be taken in accounting for this, as a recent *Hubble Space Telescope* (*HST*) study of ULIRGs (Farrah et al. 2001) found that the optical emission was in most cases dominated by old stellar populations and not by light from a starburst or AGN. The range in possible optical/near-IR SEDs for evolved stellar populations is very large, and in addition an obscured starburst or AGN can, in principle, contribute significantly in the optical or near-IR. Constraining the properties of the evolved stellar component in any of our sample with the limited available optical photometry therefore proved impossible. We have therefore assumed that all emission shortwards of 3.5 μm in the rest frame of the objects contains a significant but unquantified contribution from old stellar populations. As this contribution could lie between 0 and 100 per cent, any measured flux at a rest-frame wavelength shorter than 3.5 μm is treated as a 3σ upper limit in the fitting.

Table 2. Ultraluminous infrared galaxies: optical and near-IR data.

Name	*U*	*B*	*V*	*R*	*J*	*H*	*K*	*L*
00198−7926					619 ± 41	764 ± 51	565 ± 38	232 ± 15
00199−7426					1.0 ± 0.1	5.4 ± 0.6	6.4 ± 0.7	
00262+4251					5.4 ± 1.6		5.5 ± 1.6	
00335−2732				0.94 ± 0.1	4.2 ± 0.4	3.3 ± 0.3	5.0 ± 0.5	
01388−4618		0.31 ± 0.04						
02364−4751		0.44 ± 0.05						
03068−5346								
04232+1436					5.5 ± 1.6		10.6 ± 3.2	
05189−2524		0.66 ± 0.07	0.65 ± 0.07	0.76 ± 0.08	14.7 ± 0.9	30.8 ± 2.1	57.1 ± 3.8	136 ± 30
06035−7102					2.1 ± 0.2	2.8 ± 0.3	4.2 ± 0.4	
06206−6315					1.3 ± 0.1	1.7 ± 0.2	2.8 ± 0.3	
08572+3915		0.51 ± 0.05	0.65 ± 0.07	0.90 ± 0.1	1.7 ± 0.1	3.0 ± 0.2	3.9 ± 0.3	50 ± 10
09111−1007					3.4 ± 0.3	5.5 ± 0.6	7.4 ± 0.7	
09320+6134		0.96 ± 0.1	10.91 ± 1.2	1.11 ± 0.1	12.9 ± 0.9	21.2 ± 1.4	29.2 ± 1.9	33 ± 7
09583+4714					1.2 ± 0.1	1.5 ± 0.2	2.0 ± 0.2	
10035+4852								
10190+1322					2.3 ± 0.2	3.0 ± 0.3	2.1 ± 0.2	
10494+4424					1.0 ± 0.1	2.0 ± 0.2	2.8 ± 0.3	
10565+2448					14.0 ± 1.4	17.0 ± 1.7	18.0 ± 1.8	
12112+0305		0.16 ± 0.02	0.25 ± 0.03	0.32 ± 0.03	2.0 ± 0.2	2.9 ± 0.3	3.5 ± 0.4	2.2 ± 0.5
12540+5708	2.77 ± 0.5	7.34 ± 1.24	13.1 ± 2.2	11.5 ± 0.1	49 ± 3	107 ± 7	186 ± 12	368 ± 72
13428+5608		0.74 ± 0.07	1.03 ± 0.1	1.76 ± 0.2	9.0 ± 0.9	13.5 ± 1.4	16.1 ± 1.6	17.4 ± 1.7
14348−1447		0.22 ± 0.02	0.24 ± 0.02	0.43 ± 0.04	1.7 ± 0.2	2.5 ± 0.3	3.3 ± 0.3	
14378−3651					2.5 ± 0.3	2.8 ± 0.3	5.0 ± 0.5	
15250+3609		0.26 ± 0.03	0.27 ± 0.03	0.42 ± 0.04	3.1 ± 0.3	4.0 ± 0.4	4.1 ± 0.4	4.0 ± 0.4
15327+2340		0.96 ± 0.1	3.16 ± 0.3	4.07 ± 0.4	9.6 ± 1.0	17.9 ± 1.8	23.0 ± 2.3	22.7 ± 2.3
17132+5313					5.6 ± 0.6	8.2 ± 0.8	8.9 ± 0.9	10.5 ± 1.6
17208−0014								
18470+3233					2.7 ± 0.4		3.6 ± 0.5	
19254−7245								
19297−0406								
19458+0944								
20046−0623					3.9 ± 0.6		4.0 ± 0.6	
20414−1651								
20551−4250		3.93 ± 0.34		5.04 ± 0.34	22.9 ± 5.9	30.2 ± 7.8	25.7 ± 6.7	
21130−4446				0.89 ± 0.09				
21504−0628					5.5 ± 0.8		5.7 ± 0.9	
22491−1808		0.22 ± 0.02	0.20 ± 0.02	0.26 ± 0.03	2.1 ± 0.2	2.7 ± 0.3	2.6 ± 0.3	2.4 ± 0.2
23128−5919		4.09 ± 0.4		7.69 ± 0.7	9.6 ± 0.6	12.6 ± 0.8	11.9 ± .08	
23365+3604					7.5 ± 0.4		6.5 ± 0.3	
23389−6139		0.35 ± 0.04						

All fluxes are given in mJy and are in the observed frame. 1σ errors are quoted.

4.2 Star formation rates

Estimating obscured star formation rates from IR data is based on silicate and graphite dust grains absorbing the optical and UV light from young stars and reradiating at IR and submillimetre wavelengths. A recent estimate for deriving star formation rates from IR luminosities has been made by Rowan-Robinson et al. (1997):

$$\dot{M}_{*,\mathrm{all}} = 2.6 \times 10^{-10} \frac{\phi}{\epsilon} \frac{L_{60}}{\mathrm{L}_{\odot}}, \quad (1)$$

where $\dot{M}_{*,\mathrm{all}}$ is the star formation rate, ϵ is the fraction of optical/UV light from the starburst that is absorbed by dust and re-emitted in the IR, and L_{60} is the 60-μm starburst luminosity. The factor ϕ incorporates the correction between a Salpeter initial mass function (IMF) and the true IMF (×1.0 for a Salpeter IMF, ×3.3 for a Miller–Scalo IMF), and a correction for the assumed upper and lower stellar mass bounds for the stars forming in the starburst (×1.0 if the mass range is $0.1 < \mathrm{M}_{\odot} < 100$, ×0.323 if the mass range spans only OBA-type stars, i.e. $1.6 < \mathrm{M}_{\odot} < 100$). We have assumed that all of the optical/UV light from the starburst is absorbed ($\epsilon \sim 1.0$), and that the IMF of the starburst is a Salpeter IMF forming stars across the mass range $0.1 < \mathrm{M}_{\odot} < 100$ ($\phi = 1.0$). The star formation rates for our sample calculated using equation (1) are given in Table 4.

4.3 Dust masses and temperatures

The starburst and AGN models do not assume a monolithic dust temperature, but instead invoke a range of dust temperatures spanning 10–1000 K. An estimate of the mass-weighted mean dust temperature can be obtained by fitting an optically thin greybody function of the form

$$S_{\nu} = \nu^{\beta} B(\nu, T_{\mathrm{dust}}) \quad (2)$$

to the far-infrared (FIR) SED over the wavelength range 200–1000 μm, which measures the colour temperature of the system. In equation (2), S_{ν} is the source flux at a frequency ν, T_{dust} is the dust

Table 3. Ultraluminous infrared galaxies: mid-IR, far-IR and submillimetre fluxes.

Name	5.9	7.7	10	12	15	25	60	90	100	120	150	180	200	450	850	1100
00198−7926				277		1149	3104		2870							
00199−7426			57.0	100		326	4157		6148	7500	5340	4210	3000			
00262+4251	5.6	73.9	<87	43.0		335	2983	2600	2438	2900	2400	2400	<2100			
00335−2732				60.0		632	4294		3207							
01388−4618	11.2	84.9		100		353	2914		3695							
02364−4751	70.0	65.1		50.0		175	2794		4953							
03068−5346			<63	40.0	50.0	195	3417	3340	3955	3330	2780	1720	1350			
04232+1436			<108	65.0	70.0	390	3449	4140	4256	3500	2300	1600	1100			
05189−2524			600	729	1000	3444	13670	10700	11360	10000	6800	4360	3840		<110	30.0
06035−7102	48.9	158	90.0	116	150	574	5127	5050	5651	5150	2900	2010	1350			
06206−6315	12.3	67.5	<72	40.0	110	294	3959	4200	4577	4570	2900	1870	1500			
08572+3915			260	318		1703	7433		4588					<1210	17.0	<26.2
09111−1007				167		473	7079		11060							
09320+6134	59.0	274	107	250		1034	11540		20230					1433		68.0
09583+4714				< 85		482	2643		3061							
10035+4852				98.4		283	4593		6242							
10190+1322				120		379	3328		5574							
10494+4424				60.0		165	3527		5412							
10565+2448			182	217	270	1138	12120		15130					533	61.0	
12112+0305	16.8	107	65.0	100	200	509	8503	8950	9976	8310	5870	3930	2930	281	49.0	15.0
12540+5708	606	1208	1425	1872	2900	8662	31990	27340	30290	24320	14740	9750	6880	513		46.9
13428+5608	76.2	294	100	235	500	2282	21740	23780	21380	19990	13100	8690	7400	707		51.0
14348−1447	12.6	85.9	<96	108	<270	495	6870	7230	7068	6660	5610	3760	2690	217	24.0	17.0
14378−3651			<276	< 116	<360	525	6194	7490	6342	5900	3600	2800	2450			
15250+3609	28.0	173	<267	238		1323	7286	6660	5907	4160	2370	1600	1160	252	33.0	29.6
15327+2340		583	147	483.7	1140	7907	103800	111500	112400	109000	87890	63950	54810	6286	832	350
17132+5313			84.0	121.7		620	5678		8043							
17208−0014	32.2	223					17900		19400					1070	155	
18470+3233				135	150	425	4071	3550	3432	3200	2450	1700	1250			
19254−7245	88.8	150	123	120	342	1242	5484	5260	5789	4270	3060	2300	1610			
19297−0406				110		589	7052		7719							
19458+0944	7.0	53.4	<396	150	<770	260	3950	5820	7110		7610		7050			
20046−0623			<84	125	<390	470	3338	4710	4060	3690	3180.	2790	1400	<160	<26	
20414−1651			<168	80.0	<180	346	4364	4220	5247	3600	2560	1540	<1350			
20551−4250	45.3	232	<204	284	500	1906	12780	9260	9948	6730	4140	2560	1800			
21130−4446			<90	55.0	<450	150	3106	3600	3782	4500	3940	3140	2900			
21504−0628			40.0	50.0	150	388	3483	2820	2886	2800	1520	1260	700	<110	<16	
22491−1808	8.4	59.3	<39	80.0	110	550	5436	5450	4453	3550	2700	1950	1700	<200	19.0	
23128−5919	41.7	230	126	245	360	1590	10800	11360	10990	10000	6400	4700	3500			
23365+3604	12.6	106	<120	80.0	150	808	7087	6760	8363	6750	4810	3350	3010	170	20.0	
23389−6139		28.9	<75	31.0	<260	244	3628	3300	4260	4030	2830	1990	1520			

All wavelengths are in μm. All fluxes are in mJy and are in the observed frame, except the 5.9- and 7.7-μm fluxes which are in the rest frame. 1σ errors are 10 per cent on the *IRAS* fluxes, 20 per cent on the 5.9-, 7.7-, 10- and 15-μm fluxes, 30 per cent on all other IR fluxes up to 200 μm and 20 per cent on the submillimetre fluxes.

temperature, $B(\nu, T_{\rm dust})$ is the Planck function and β is the frequency dependence of the grain emissivity. Monolithic dust temperatures derived in this way are unphysical simplifications in AGN, but can serve as a useful comparison with previous work. Mass-weighted mean dust temperatures for our sample are presented in Table 4.

Gas and dust masses can be estimated in two ways. The first way is to calculate the gas mass directly from the models using equation (4) of Farrah et al. (2002b). This, however, gives the total gas mass at the current age of the starburst without accounting for gas that is blown out of the nuclear regions by supernovae or superwinds, and thus may overestimate the amount of gas and dust in the system. The second approach is to estimate the dust mass directly from the submillimetre SED. An approach for estimating dust and gas masses in galaxies using submillimetre data is to assume the system is optically thin at these wavelengths, and to follow the prescription of Hildebrand (1983):

$$M_{\rm dust} = \frac{1}{1+z}\frac{S_{\nu_o} D_L^2}{\kappa(\nu_r) B(\nu_r, T_{\rm dust})}, \quad (3)$$

where ν_o and ν_r are the observed and rest frame frequencies, respectively, S_{ν_o} is the flux in the observed frame, $B(\nu_r, T_{\rm dust})$ is the Planck function in the rest frame and $T_{\rm dust}$ is the dust temperature. The gas mass is then obtained by assuming a fixed gas-to-dust ratio. For the most extreme *IRAS* galaxies, the best current estimate of the gas-to-dust ratio is 540 ± 290 (Sanders, Scoville & Soifer 1991). For comparison, the gas-to-dust ratio in spiral galaxies is thought to be ∼500 (Devereux & Young 1990), and ∼700 in ellipticals (Wiklind & Henkel 1995). The mass absorption coefficient in the rest frame, κ_r, is taken to be

$$\kappa_r = 0.067\left(\frac{\nu_r}{2.5\times10^{11}}\right)^{\beta} \quad (4)$$

in units of $\rm m^2\ kg^{-1}$. Dust masses and temperatures calculated using equations (2) and (3) are given in Table 4.

5 INDIVIDUAL OBJECTS

In this section we present further discussion on objects in our sample that are either well-studied by previous authors, or that show interesting or unusual features.

00198−7926. This source is a double-nucleus system with a large tail, with a Sy2 optical spectrum. The second nucleus is probably a large region of extranuclear unobscured star formation, and there are a number of H II regions embedded in the tail (Heisler & Vader 1994). A deep *Bepposax* observation gave no detection, giving an upper limit to the X-ray flux of $F_{2-10} < 1\times10^{-13}$ erg $\rm cm^{-2}\ s^{-1}$ (Risaliti et al. 2000). From our results, the properties of this object mark it as unusual. We find that the IR emission from this object is mostly starburst in origin. The starburst is comparatively old, and can thus account for both the submillimetre emission and all of the unobscured star formation observed by Heisler & Vader (1994). We interpret the 'warm' infrared colour of this object as being due to the old starburst rather than an AGN. There is, however, comparatively little IR data available for this object and the resulting AGN upper limit is weak. The best-fitting model, shown in Fig. 1, includes an AGN component.

05189−2524. This object appears to be a late-stage merger. It possesses a single, compact, very red nucleus with a Sy2 spectrum (Veilleux et al. 1995), bisected by a dust lane (Scoville et al. 2000). Young et al. (1996) observed broad lines in polarized flux in this object, suggesting the presence of an obscured AGN. Later observations (Dudley 1999) observed the 11.3-μm dust feature, suggesting that this object also contains a buried starburst. The X-ray spectrum (Risaliti et al. 2000) is well fitted by a two-component model, consisting of a power law with $\Gamma = 1.89^{+0.35}_{-0.34}$, absorbed by a column density of $N_{\rm H} = 4.7^{+1.4}_{-1.1}$ $\rm cm^{-2}$, and a thermal component with $kT = 0.88^{+0.89}_{-0.35}$ keV. Overall the power-law component can be interpreted as arising from a Compton thin AGN, with the thermal component either due to the AGN or to starburst activity. For our SED fitting we compiled an additional *N*-band (10.6 μm) flux of 498 ± 100 mJy from Maiolino et al. (1995). From our results, we find that this object contains both a starburst and an AGN, where the AGN provides a significant fraction of the total IR luminosity.

09320+6134. This object possesses a single bright nucleus and a disturbed spiral structure (Scoville et al. 2000). There is one large tail extending ∼38 kpc, and a second tail that forms almost a complete ring with a total length of ∼65 kpc. The morphology has been interpreted as a late-stage merger between two large spiral galaxies (Sanders et al. 1988), possibly involving a third gas-poor dwarf galaxy (Majewski et al. 1993). The optical spectrum is a combination of a LINER and a Sy2 (Gonçalves, Véron-Cetty & Véron 1999). Near-IR spectroscopy by Imanishi, Dudley & Maloney (2001) shows that this object is likely to contain a heavily obscured AGN. Conversely, Lutz, Veilleux & Genzel (1999) classify this object as starburst powered on the basis of mid-IR spectroscopy, and the submillimetre emission is also consistent with a starburst (Rigopoulou et al. 1996). We compiled an additional 350-μm upper limit of 2664 mJy, and an additional 800-μm flux of 143 ± 25 mJy from Rigopoulou et al. (1996). We find that this system is a composite object containing both a starburst and an AGN, a result that is consistent with previous observations. From the SED fit presented in Fig. 1 it can be seen that the AGN has a higher near-IR flux than the starburst component, but that the AGN contribution in the mid-IR is small, and is negligible in the submillimetre. This object is a case in point that, in order to understand the power source in ULIRGs it is necessary to have data spanning a wide wavelength range.

10565+2448. We compiled an additional 350-μm flux of 1240 ± 248 mJy, and a 750-μm flux of 85 ± 17 mJy from Rigopoulou et al. (1996). The AGN in this object, although weak compared with the starburst, is required for an acceptable SED fit.

12112+0305. This system contains two separate nuclei with a pair of tidal tails (Scoville et al. 2000). The optical spectrum is that of a LINER (Veilleux et al. 1999). This source is classified as a starburst on the basis of its mid-IR spectrum (Rigopoulou et al. 1999). We compiled an additional 800-μm flux of 50 ± 13 mJy from Rigopoulou et al. (1996). The extensive IR data available for this object allow us to place strong constraints on the power source. We find that this object is powered by a starburst, with a severe upper limit on any AGN contribution.

12540+5708. This galaxy is commonly known as Mrk 231 and has a Sy1 optical spectrum. The IR luminosity is thought to be powered by both starburst and AGN activity (Cutri, Rieke & Lebofsky 1984; Condon et al. 1991). Mrk 231 possesses a single compact nucleus surrounded by irregular 'rings' of recent star formation and a small tidal arm containing numerous blue star-forming 'knots', and is therefore thought to be an advanced merger. The nucleus is unresolved in the radio band (Condon et al. 1991) and at 11.7 μm (Miles et al. 1996), implying that the emission from the nucleus is powered by an AGN rather than a starburst. Mrk 231 is classified as an AGN on the basis of both near-IR spectroscopy (Imanishi et al. 2001) and mid-IR spectroscopy (Rigopoulou et al. 1999). Conversely, the X-ray emission from this object, although weak, cannot

Table 4. Ultraluminous galaxies: luminosities and model parameters.

Name	$\chi^{2,a}$	$L_{\rm IR}^{\rm Tot}$ ($L_\odot$)	$L_{\rm IR}^{\rm Sb}$ ($L_\odot$)	$L_{\rm IR}^{\rm AGN}$ ($L_\odot$)	Age^b (Myr)	SFR^c ($M_\odot$ yr^{-1})	θ^d (°)	M_d^e ($M_\odot$)	T^f (K)	β^g
00198−7926	3.50	$12.72^{+0.01}_{-0.02}$	$12.65^{+0.05}_{-0.03}$	<11.91	64–71	130 ± 50	–	$7.31^{+0.15}_{-0.10}$	36 ± 4	1.95 ± 0.22
00199−7426	2.35	$12.36^{+0.02}_{-0.02}$	$12.30^{+0.04}_{-0.01}$	$11.34^{+0.11}_{-0.17}$	26-37	360 ± 50	–	$8.48^{+0.09}_{-0.12}$	27 ± 7	1.96 ± 0.40
00262+4251	1.66	$12.10^{+0.01}_{-0.01}$	$11.64^{+0.08}_{-0.01}$	$11.92^{+0.01}_{-0.06}$	26–45	50 ± 30	<15	$8.42^{+0.20}_{-0.50}$	25 ± 5	1.87 ± 0.05
00335−2732	1.33	$12.01^{+0.04}_{-0.04}$	$11.99^{+0.03}_{-0.04}$	<10.95	<57	170 ± 20	–	$7.07^{+0.09}_{-0.02}$	42 ± 3	1.97 ± 0.20
01388−4618	2.08	$12.11^{+0.03}_{-0.04}$	$12.03^{+0.03}_{-0.04}$	<11.35	>26	200 ± 20	–	$8.10^{+0.09}_{-0.17}$	28 ± 4	1.92 ± 0.10
02364−4751	1.93	$12.20^{+0.01}_{-0.01}$	$12.15^{+0.01}_{-0.02}$	$11.23^{+0.07}_{-0.10}$	>10	260 ± 30	–	$7.97^{+0.02}_{-0.03}$	32 ± 7	1.91 ± 0.20
03068−5346	1.56	$11.96^{+0.01}_{-0.02}$	$11.93^{+0.04}_{-0.03}$	<10.94	1.6–6.6	180 ± 40	–	$7.62^{+0.09}_{-0.12}$	35 ± 3	1.97 ± 0.20
04232+1436	1.41	$12.07^{+0.03}_{-0.04}$	$11.95^{+0.10}_{-0.11}$	<11.70	<37	210 ± 30	–	$7.87^{+0.11}_{-0.30}$	31 ± 4	1.90 ± 0.25
05189−2524	2.20	$12.16^{+0.04}_{-0.02}$	$11.99^{+0.06}_{-0.06}$	$11.67^{+0.07}_{-0.12}$	6.6–26	170 ± 30	25–54	$7.61^{+0.28}_{-0.20}$	33 ± 5	1.94 ± 0.06
06035−7102	1.00	$12.24^{+0.01}_{-0.02}$	$12.19^{+0.01}_{-0.05}$	$11.21^{+0.20}_{-0.05}$	16–26	290 ± 30	>25	$7.74^{+0.04}_{-0.05}$	35 ± 2	1.95 ± 0.03
06206−6315	1.00	$12.21^{+0.01}_{-0.01}$	$12.18^{+0.01}_{-0.06}$	$11.05^{+0.40}_{-0.23}$	16–26	300 ± 30	<45	$7.93^{+0.02}_{-0.04}$	31 ± 2	1.92 ± 0.02
08572+3915	2.22	$12.17^{+0.01}_{-0.01}$	$11.99^{+0.01}_{-0.06}$	$11.70^{+0.09}_{-0.02}$	<57	180 ± 20	–	$7.04^{+0.20}_{-0.06}$	45 ± 5	1.92 ± 0.10
09111−1007	1.92	$12.01^{+0.02}_{-0.02}$	$12.01^{+0.02}_{-0.03}$	<10.64	26–37	192 ± 25	–	$7.90^{+0.11}_{-0.16}$	29 ± 4	1.94 ± 0.28
09320+6134	2.11	$12.01^{+0.01}_{-0.01}$	$11.98^{+0.01}_{-0.01}$	$10.86^{+0.03}_{-0.10}$	>16	160 ± 20	>25	$8.33^{+0.04}_{-0.11}$	25 ± 3	1.93 ± 0.03
09583+4714	1.00	$12.06^{+0.05}_{-0.06}$	$11.90^{+0.12}_{-0.10}$	<11.80	–	160 ± 70	–	–	34 ± 15	1.95 ± 0.70
10035+4852	1.00	$11.98^{+0.04}_{-0.05}$	$11.97^{+0.05}_{-0.07}$	<11.50	–	180 ± 30	–	$7.87^{+0.10}_{-0.15}$	29 ± 5	1.95 ± 0.20
10190+1322	1.00	$12.10^{+0.03}_{-0.02}$	$12.01^{+0.03}_{-0.03}$	$11.36^{+0.08}_{-0.13}$	<16	195 ± 15	–	$7.85^{+0.05}_{-0.05}$	32 ± 3	1.97 ± 0.15
10494+4424	2.04	$12.20^{+0.02}_{-0.02}$	$12.16^{+0.02}_{-0.02}$	<11.06	<26	280 ± 40	–	$7.97^{+0.05}_{-0.05}$	32 ± 5	1.94 ± 0.26
10565+2448	1.23	$12.06^{+0.02}_{-0.02}$	$12.03^{+0.03}_{-0.02}$	$10.80^{+0.14}_{-0.10}$	26–37	200 ± 20	–	$7.85^{+0.05}_{-0.07}$	30 ± 2	1.95 ± 0.20
12112+0305	2.30	$12.29^{+0.02}_{-0.02}$	$12.29^{+0.02}_{-0.03}$	<9.50	16–26	390 ± 20	–	$7.94^{+0.08}_{-0.13}$	33 ± 2	1.95 ± 0.10
12540+5708	1.56	$12.58^{+0.04}_{-0.03}$	$12.42^{+0.06}_{-0.06}$	$12.05^{+0.10}_{-0.01}$	10–16	470 ± 50	27–54	$7.95^{+0.02}_{-0.17}$	36 ± 2	1.94 ± 0.01
13428+5608	1.99	$12.15^{+0.04}_{-0.03}$	$12.09^{+0.06}_{-0.03}$	$11.21^{+0.05}_{-0.50}$	16–26	260 ± 30	–	$7.70^{+0.17}_{-0.02}$	31 ± 4	1.95 ± 0.08
14348−1447	1.98	$12.30^{+0.01}_{-0.03}$	$12.18^{+0.04}_{-0.04}$	$11.54^{+0.12}_{-0.25}$	26–37	310 ± 30	<32	$7.97^{+0.02}_{-0.02}$	32 ± 1	1.91 ± 0.02
14378−3651	1.00	$12.12^{+0.03}_{-0.02}$	$12.03^{+0.10}_{-0.01}$	<11.36	16–26	250 ± 40	–	$7.81^{+0.05}_{-0.20}$	34 ± 5	1.95 ± 0.3
15250+3609	2.32	$12.08^{+0.03}_{-0.04}$	$11.68^{+0.08}_{-0.08}$	$11.86^{+0.07}_{-0.10}$	10–37	70 ± 30	<15	$7.43^{+0.08}_{-0.12}$	37 ± 4	1.69 ± 0.1
15327+2340	2.01	$12.14^{+0.02}_{-0.01}$	$12.14^{+0.02}_{-0.01}$	<9.90	26–37	240 ± 30	–	$8.32^{+0.05}_{-0.06}$	27 ± 3	1.93 ± 0.02
17132+5313	1.00	$11.92^{+0.03}_{-0.01}$	$11.84^{+0.02}_{-0.01}$	$11.14^{+0.01}_{-0.11}$	10–26	130 ± 20	–	$7.64^{+0.18}_{-0.05}$	31 ± 3	1.95 ± 0.03
17208−0014	4.70	$11.99^{+0.03}_{-0.04}$	$11.99^{+0.04}_{-0.05}$	<11.00	>16	150 ± 30	–	$8.25^{+0.19}_{-0.25}$	26 ± 6	1.95 ± 0.3
18470+3233	1.00	$12.08^{+0.03}_{-0.04}$	$12.03^{+0.04}_{-0.04}$	<11.42	6.6–37	200 ± 40	–	$7.54^{+0.31}_{-0.30}$	35 ± 6	1.95 ± 0.05
19254−7245	1.52	$12.24^{+0.08}_{-0.10}$	$12.17^{+0.10}_{-0.05}$	<11.60	–	170 ± 50	–	$7.60^{+0.11}_{-0.14}$	34 ± 4	1.96 ± 0.1
19297−0406	1.00	$12.41^{+0.02}_{-0.05}$	$12.39^{+0.03}_{-0.06}$	<11.50	<57	480 ± 150	–	$8.15^{+0.10}_{-0.15}$	31 ± 6	1.95 ± 0.25
19458+0944	1.73	$12.40^{+0.01}_{-0.02}$	$12.25^{+0.03}_{-0.01}$	$11.83^{+0.04}_{-0.08}$	∼26	280 ± 30	–	$8.99^{+0.03}_{-0.12}$	22 ± 2	1.89 ± 0.01
20046−0623	1.00	$12.17^{+0.03}_{-0.04}$	$12.11^{+0.03}_{-0.11}$	<11.60	<26	210 ± 60	–	$7.86^{+0.02}_{-0.18}$	32 ± 9	1.96 ± 0.55
20414−1651	1.18	$12.22^{+0.01}_{-0.02}$	$12.16^{+0.01}_{-0.01}$	$11.31^{+0.05}_{-0.10}$	6.6–16	300 ± 15	–	$7.49^{+0.16}_{-0.14}$	38 ± 2	1.96 ± 0.10
20551−4250	1.95	$12.05^{+0.04}_{-0.05}$	$11.90^{+0.01}_{-0.10}$	$11.53^{+0.03}_{-0.17}$	10–57	160 ± 20	–	$7.05^{+0.13}_{-0.05}$	44 ± 3	1.91 ± 0.04
21130−4446	1.65	$12.14^{+0.02}_{-0.01}$	$12.11^{+0.03}_{-0.02}$	<10.90	37–64	250 ± 15	–	$7.99^{+0.05}_{-0.03}$	30 ± 2	1.94 ± 0.10
21504−0628	1.00	$12.00^{+0.03}_{-0.04}$	$11.94^{+0.04}_{-0.07}$	$11.06^{+1/4}_{-0.15}$	<57	180 ± 20	–	$7.15^{+0.11}_{-0.15}$	42 ± 4	1.97 ± 0.10
22491−1808	2.38	$12.16^{+0.01}_{-0.02}$	$11.61^{+0.02}_{-0.07}$	$12.02^{+0.03}_{-0.03}$	∼26	60 ± 10	<10	$8.04^{+0.03}_{-0.04}$	27 ± 3	1.80 ± 0.02
23128−5919	2.15	$12.02^{+0.02}_{-0.02}$	$11.93^{+0.04}_{-0.07}$	$11.30^{+0.10}_{-0.07}$	26–37	150 ± 30	–	$7.75^{+0.07}_{-0.08}$	30 ± 3	1.93 ± 0.03
23365+3604	2.90	$12.19^{+0.01}_{-0.01}$	$12.00^{+0.01}_{-0.02}$	$11.73^{+0.02}_{-0.09}$	∼26	200 ± 20	<10	$7.81^{+0.02}_{-0.03}$	33 ± 2	1.86 ± 0.02
23389−6139	1.22	$12.16^{+0.01}_{-0.01}$	$12.15^{+0.01}_{-0.02}$	$10.48^{+0.12}_{-0.18}$	16–26	290 ± 30	–	$7.70^{+0.20}_{-0.09}$	33 ± 4	1.94 ± 0.05

Luminosities are the logarithm of the 1–1000 μm luminosities obtained from the best-fitting combined starburst/AGN model, in units of bolometric solar luminosities. [a]Reduced χ^2 of the combined SED fit. [b]Starburst age. [c]Star formation rate. [d]Viewing angle of the AGN dust torus. [e]Dust mass. [f]Dust temperature. [g]Emissivity index.

be fitted with a pure power-law or thermal bremsstrahlung model (Iwasawa 1999). We compiled additional mid-IR data from Rieke (1976) and additional submillimetre data from Rigopoulou et al. (1996) and Carico et al. (1988). We find that Mrk 231 contains both a luminous starburst and an AGN, where the starburst contributes ∼70 per cent of the 1–1000 μm IR luminosity. Interestingly, this result is in excellent agreement with independent estimates of the starburst and AGN luminosities in Mrk 231 derived from very-long

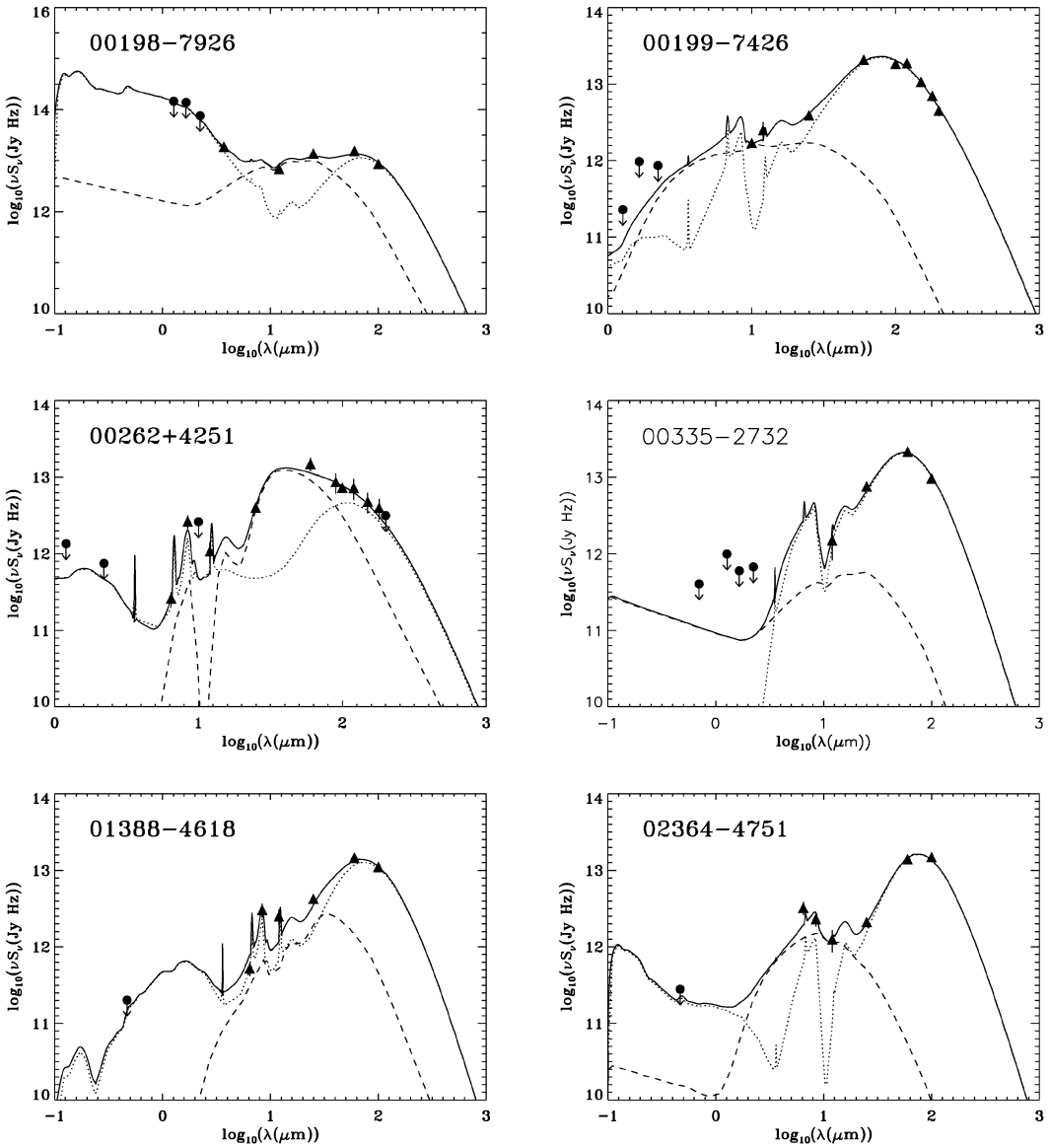

Figure 1. Best-fitting spectral energy distributions for the 41 ULIRGs in our sample. In each case the solid line is the combined best-fitting model, the dotted line is the Starburst component and the long dashed line is the AGN component.

baseline interferometry (VLBI) observations (Lonsdale et al. 2003). From Fig. 1 we can see that the AGN dominates the emission in the near- and mid-IR, in agreement with results of previous authors, but that the starburst dominates at submillimetre wavelengths.

13428+5608. This object is commonly known as Mrk 273. It contains two nuclei with a single, long (41-kpc) tidal tail and a 'ring' of star formation almost 100 kpc in diameter. The northern nucleus is resolved and is surrounded by unobscured star formation, whereas the southern nucleus is redder and unresolved (Scoville et al. 2000). The optical spectrum is that of a Sy2, and there are no broad lines in the near-IR spectrum, although there are strong narrow lines (Veilleux et al. 1999). Radio continuum and H I 21-cm observations of this source classify it as a pure starburst (Condon et al. 1991; Carilli & Taylor 2000). Conversely, mid-IR spectral observations (Lutz et al. 1999; Rigopoulou et al. 1999) classify it as an AGN. This object is a strong X-ray source, with a complex spectrum. The best fit is a four-component model, consisting of a direct and scattered AGN power law, a thermal component and an iron line. Furthermore, the X-ray emission appears extended rather than unresolved (Levenson, Weaver & Heckman 2001). We compiled an additional 350-μm flux of 1004 ± 230 mJy, and an additional 800-μm flux of 84 ± 22 mJy, both from Rigopoulou et al. (1996). Our results are consistent with Mrk 273 containing both a starburst and an AGN, in agreement with X-ray observations. The SED fit in Fig. 1 is consistent with a starburst interpretation in the near-IR, and also gives a good fit in the mid-IR although the fit predicts that the mid-IR emission is due to a starburst rather than an AGN.

14348−1447. We compiled an additional 800-μm flux of 29 ± 10 mJy from Rigopoulou et al. (1996). This object is very luminous, where the luminosity is dominated by a starburst. Whilst this object does contain a luminous AGN, the AGN only contributes ∼17 per cent of the total infrared flux.

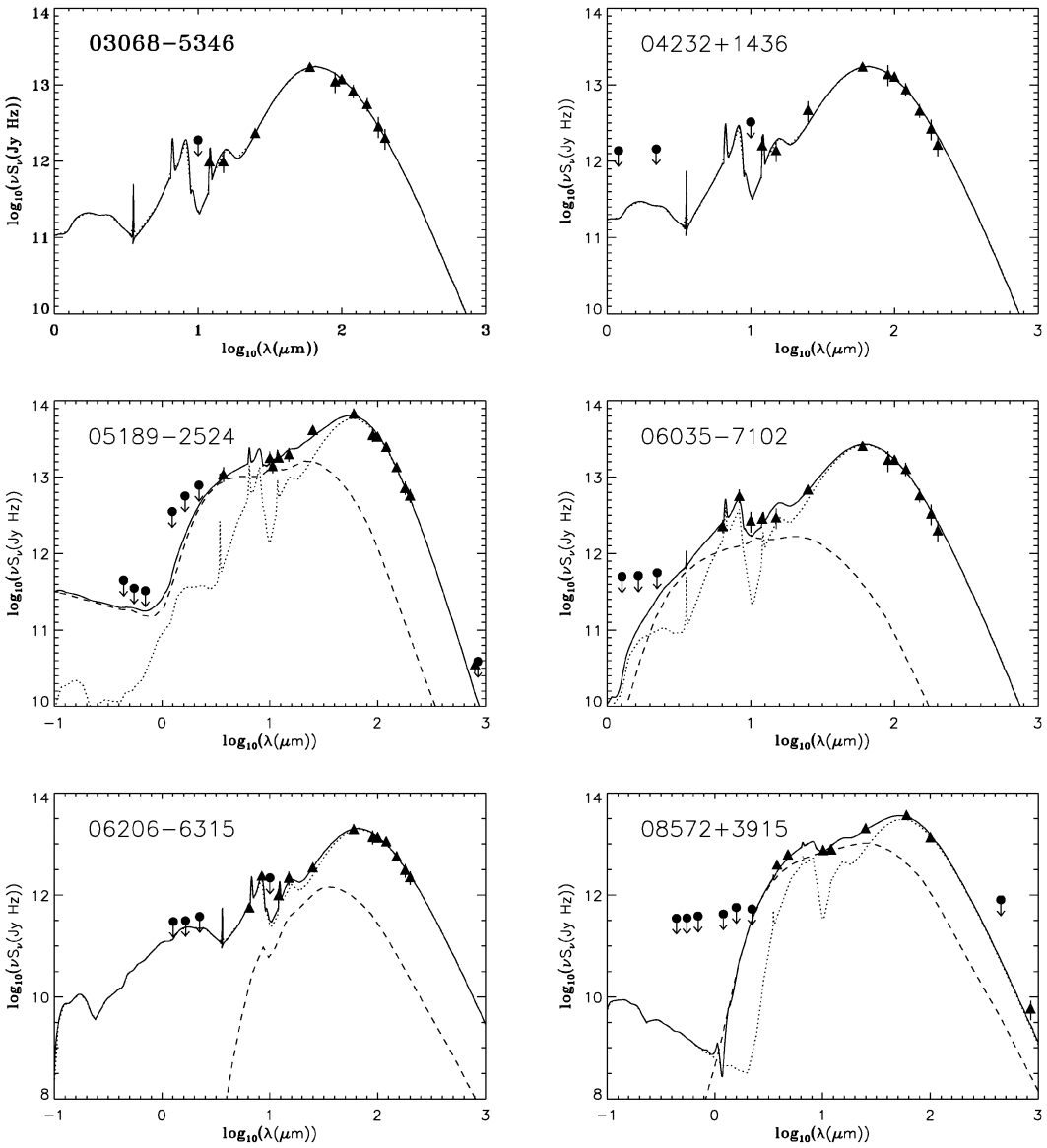

Figure 1 – *continued*

15250+3609. This object has one bright central nucleus, and a second, much dimmer nucleus 0.7 arcsec from the centre. There is also a large ring-like structure 25 kpc in diameter (Scoville et al. 2000). The optical spectrum is a composite of H II and LINER features (Veilleux et al. 1999). Lutz et al. (1999) classify this object as a starburst based on its mid-IR spectrum. Our results, however, show that this object contains both a starburst and an AGN. This is one of only three objects in the sample where the AGN provides more than half of the total IR emission. Interestingly, it can be seen from Fig. 1 that the submillimetre emission from this object is not dominated by a starburst, but instead arises in almost equal parts from a starburst and an AGN. We interpret this as arising from a heavily obscured AGN that is oriented nearly edge on to us, rather than an AGN with an extended torus.

15327+2340. This object, commonly known as Arp220, is both the closest ULIRG to us and the most intensely studied. The optical spectrum was first thought to be Sy2-like (Sanders et al. 1988), and this was interpreted as indicating an AGN power source. Conversely, the broad-band optical-IR SEDs suggested a starburst as the main power source (Joseph & Wright 1985). Observations and modelling at other wavelengths revealed a more complex picture. Ground-based mid-IR spectroscopy (Smith, Aitken & Roche 1989) suggested a hybrid nature for Arp220, including both starburst and AGN, whereas *ISO* mid-IR spectroscopy (Sturm et al. 1996) suggested a pure starburst. High-resolution VLBA imaging (Smith et al. 1998) revealed a number of unresolved sources in the nuclei, inferred to be radio supernovae, supporting the presence of a starburst. Optical integral field observations of the central regions (Arribas, Colina & Clements 2001) showed that the spectrum is LINER-like in most regions, but with a Sy2-like spectrum in the brightest emission-line region. Rieke (1988) searched for hard X-rays in Arp220 with HEAO-A1 data, and concluded that an AGN similar to those in quasars could not be the power source. Recent observations with

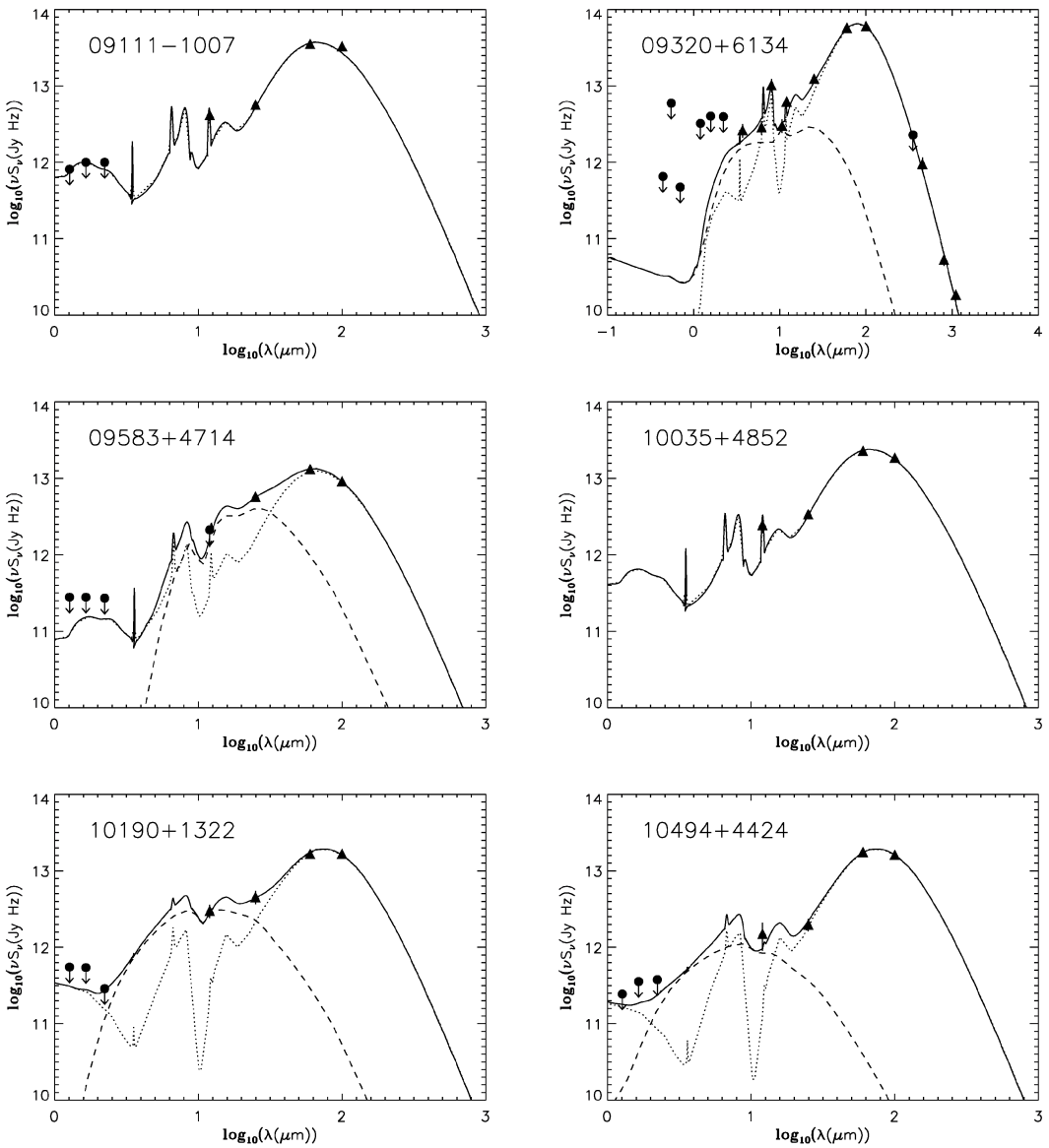

Figure 1 – *continued*

Chandra (Clements et al. 2002) detect weak hard X-ray emission from the nucleus, which has a possible origin in a weak AGN responsible for approximately 5 per cent of the bolometric luminosity. An alternative explanation, with a much larger AGN contribution to the bolometric luminosity, is possible if the AGN is obscured by a Compton-thick screen of $\sim 10^{25}$ cm^{-2} or more. There is some additional evidence for an obscured AGN in Arp220, including submillimetre observations (Haas et al. 2001) and LWS spectra that may indicate $\tau > 1$ at $\sim$100 μm (Fischer et al. 1999). We compiled additional IR photometry for Arp220 from Klaas et al. (1997), and additional submillimetre photometry from Chini et al. (1986), Rigopoulou et al. (1996) and Dunne & Eales (2001). Our results are consistent with a starburst interpretation for Arp220. The extensive IR data are well fitted by a pure starburst model, and the resulting upper limit on the IR luminosity of any AGN component is very strong. This upper limit on the AGN IR luminosity also allows us to set a lower limit in the UV optical depth of an IR luminous AGN in Arp220, of $\tau_{\rm UV} = 1500$.

17208−0014. This source has a single nucleus surrounded by a disturbed disc containing several compact star clusters, with a single tail. The optical spectrum is that of an H II region (Veilleux et al. 1999) and near-IR imaging shows an extended nucleus, arguing against an AGN (Scoville et al. 2000). This object lies in a crowded field, and high spatial resolution 100-μm observations with the Kuiper Airborne Observatory (Zink et al. 2000) measure a 100-μm flux substantially below that from *IRAS*, implying that the *IRAS* fluxes for this object are confused. The 100-μm flux used in the fit is from Zink et al. (2000). This was the only object in our sample where the fit was relatively poor ($\chi^2_{\rm red} = 4.7$), however, it can be seen from Fig. 1 that this poorness of fit is due to inconsistencies between the model and the *IRAS* 60-μm flux. As there are observed

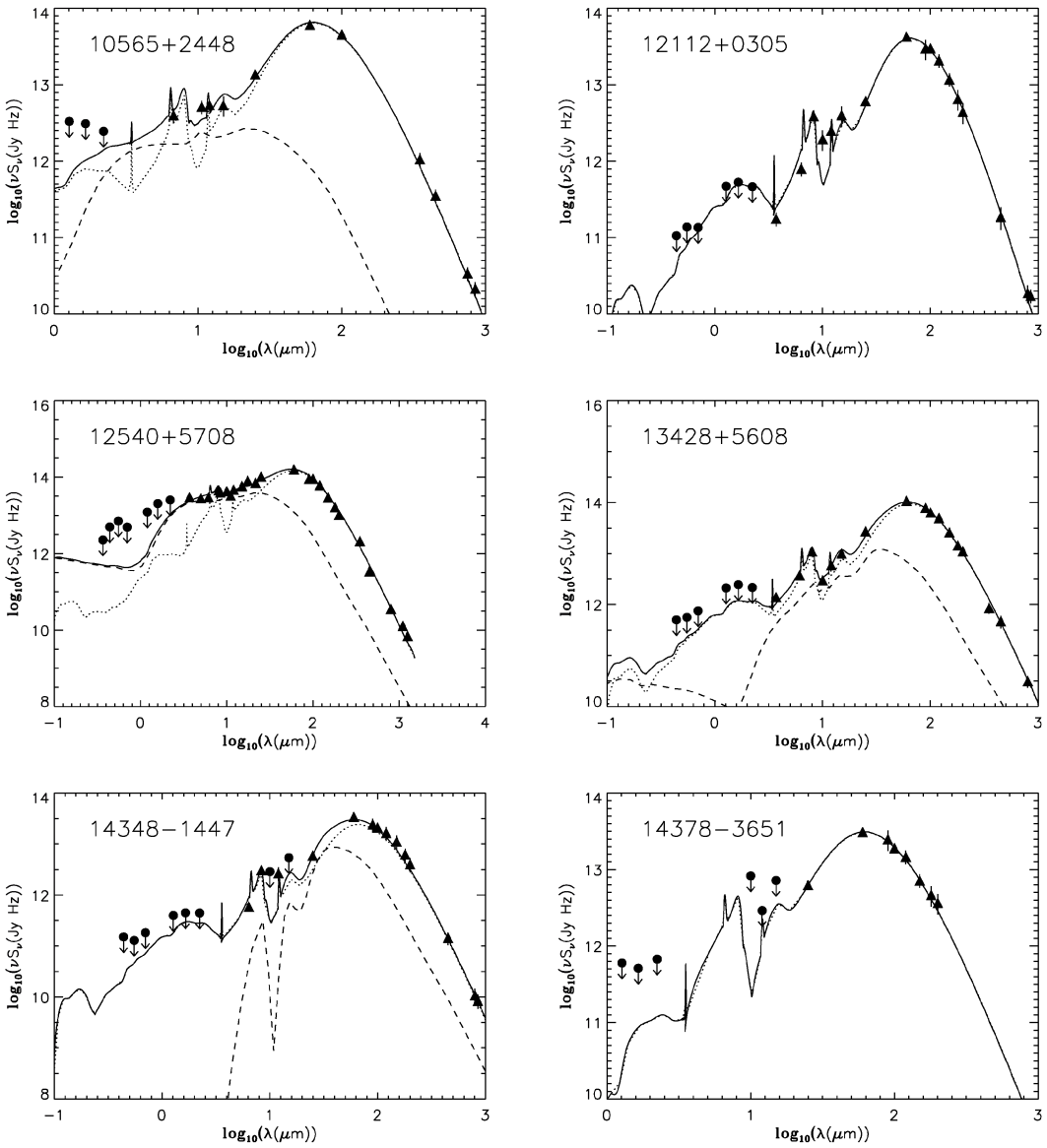

Figure 1 – *continued*

inconsistencies at 100 μm we infer that this inconsistency at 60 μm is also due to confusion. Overall, our results are consistent with a pure starburst interpretation for this object, although the AGN upper limit is weak.

19254−7245. This object is more commonly known as the Super-Antenna, and possesses a spectacular morphology. Two extremely long tail-like features extend on either side of the central regions, with a total length of 500 kpc. These features can be explained as a result of a coplanar encounter between two massive disc galaxies (Melnick & Mirabel 1990). There are two optical nuclei in the central regions, one with a Sy2 spectrum and the other with a starburst spectrum (Mirabel, Lutz & Maza 1991). Further optical spectroscopy by Colina, Lipari & Macchetto (1991) classify this source as an obscured AGN surrounded by star-forming clouds. The mid-IR spectrum of this object classifies it as an AGN (Lutz et al. 1999). X-ray observations (Pappa, Georgantopoulos & Stewart 2000) were inconclusive, but suggested an AGN was at least present in this object. We compiled for this object an extra flux at 6.7 μm of 113 ± 23 mJy from Charmandaris et al. (2002). Of our sample the SED fit for this object is of reasonable quality, but deviates markedly from one point. We interpret this as being due to the very large angular size of this object, which is much larger than any other object in our sample. Whilst *IRAS* fluxes are likely to contain all the flux from the object, it is feasible that other observations have missed some flux. Our fit (Fig. 1) is a pure starburst, but the AGN upper limit is weak.

22491−1808. This system possesses a complex morphology, with at least three possible nuclei and large numbers of star-forming 'knots'. There are also two small bright tails, in which many of the star-forming knots are embedded. Based on the morphology, Cui et al. (1991) propose a multiple merger origin for this ULIRG. The mid-IR spectrum is consistent with a starburst (Lutz et al. 1999;

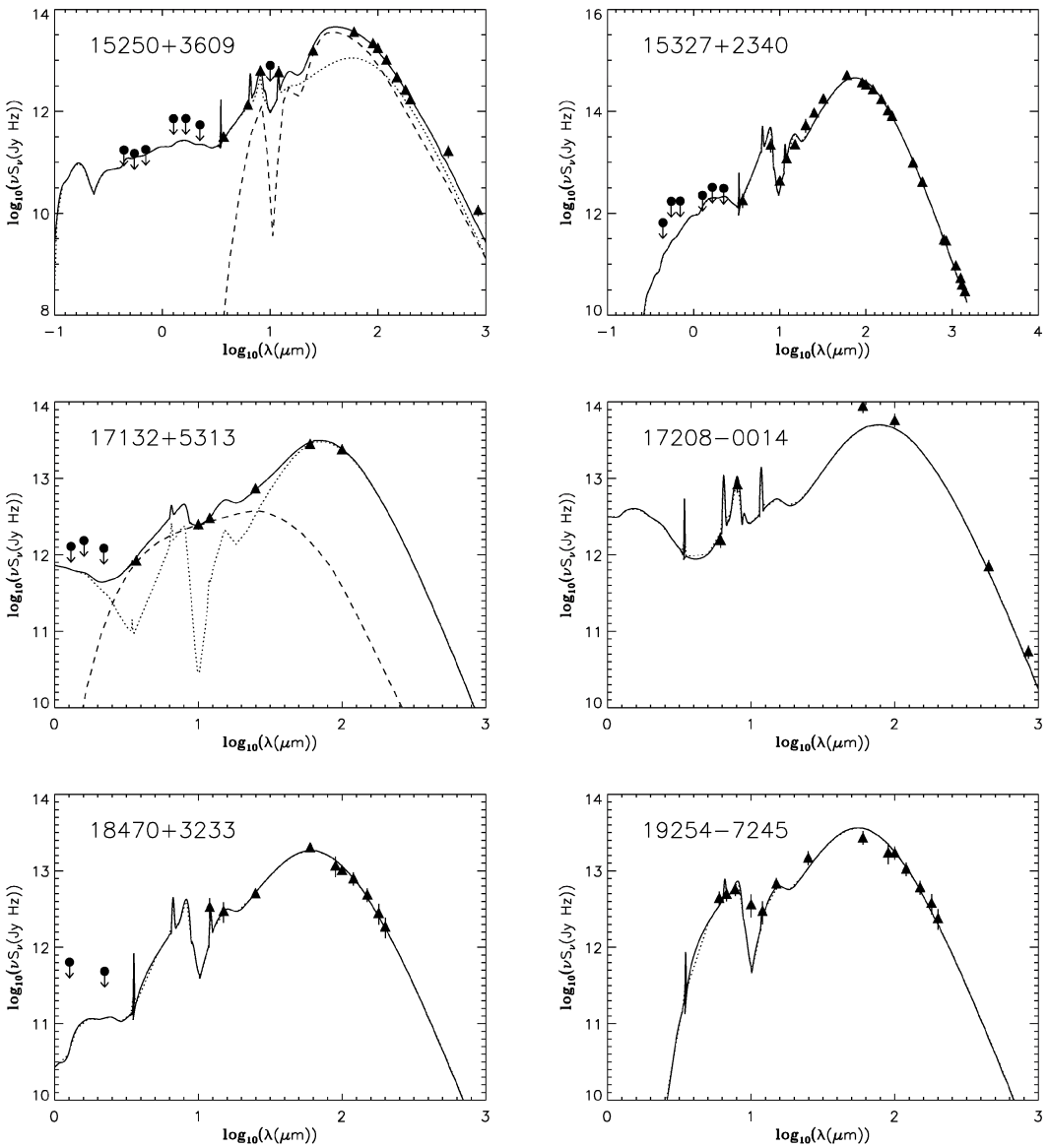

Figure 1 – *continued*

Rigopoulou et al. 1999). We, however, find that this object contains both a starburst and an AGN. This is one of only three objects where the AGN contributes more than half the total IR luminosity. In the mid-IR the starburst dominates, but with a significant AGN contribution. The contribution from the AGN in the submillimetre is comparable to the submillimetre emission from the starburst, implying that the AGN torus is being viewed almost edge on.

6 DISCUSSION

6.1 Limitations of the models

Before discussing our results, we examine the suitability of the starburst and AGN models used in this paper for understanding the nature of the power source in ULIRGs. Both sets of models are physical in nature, in that they do not assume an observational SED template for dusty star formation or AGN activity, and instead produce a predicted spectrum based on radiative transfer calculations of optical/UV light from a starburst or AGN propagating through a dusty medium. They are therefore well suited to investigating the IR emission from a population where the properties may vary markedly between individual objects. A complete description of the starburst and AGN models can be found in Efstathiou et al. (2000) and Efstathiou & Rowan-Robinson (1995), respectively.

It is, however, important to note that these models have drawbacks. In particular, the models cannot account for submillimetre emission from an extended (hundreds of parsecs instead of tens of parsecs) dust torus surrounding an AGN. If such a torus did exist in our sample the submillimetre emission from the torus could be mistakenly ascribed to star formation, leading to a substantially overestimated star formation rate. There do exist radiative transfer models for cool, extended dust surrounding an AGN. To test whether all or part of the submillimetre emission from our sample could arise from such a torus, we fitted the extended torus models of

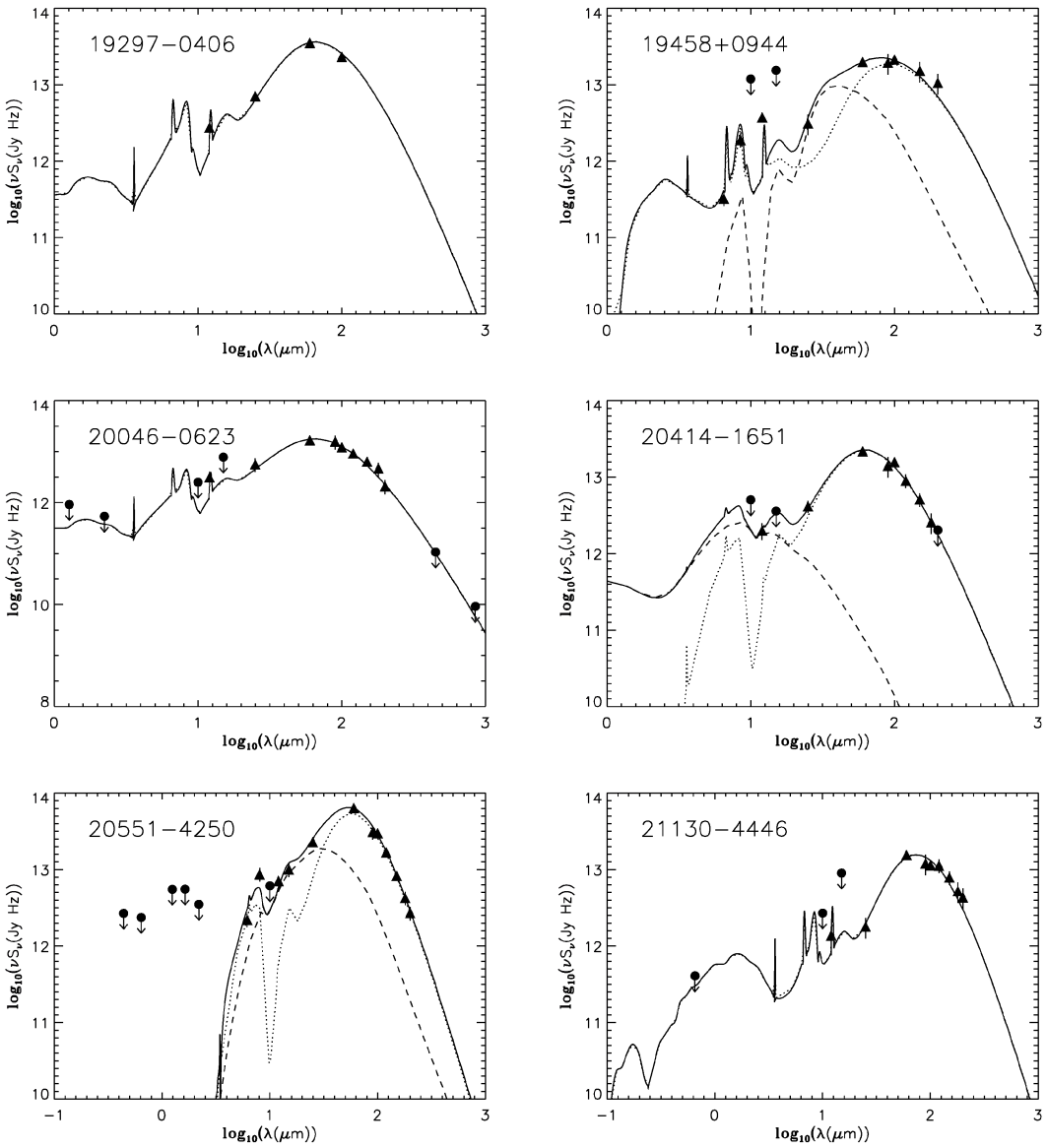

Figure 1 – *continued*

Rowan-Robinson (1995) to the objects in our sample, both on their own and in combination with the starburst models described previously. Although in all cases the extended torus models were clearly rejected, we cannot completely discount this possibility, as the extended torus models do not cover a wide range of torus geometries and lines of sight.

Despite their limitations, the models appear to work very well. In a sample of 41 objects the models produce a good fit in all but one case. As described in Section 5, in this case there is reason to believe that the relative poorness of fit may be partially due to the quality of the data. The models successfully reproduce both a wide range of ULIRG SED shapes over the wavelength range 0.4–1000 μm (if the optical data are used as upper limits), and also reproduce spectral features such as the 7.7-μm PAH line, and the 9.7-μm silicate absorption feature. We therefore find that, under the caveats described previously, these models are well suited to studying the dust-shrouded power source in ULIRGs.

6.2 Starburst and AGN activity in ULIRGs

6.2.1 What powers ultraluminous infrared galaxies?

Although ULIRGs have been studied for nearly two decades, the nature of the power source behind the IR emission has remained controversial. The most recent results on the power source in ULIRGs have come from mid-IR spectroscopy, which show that most ULIRGs (∼80 per cent) are powered mainly by starbursts (Genzel et al. 1998; Rigopoulou et al. 1999), but that at least half of local ULIRGs show evidence for both starburst and AGN activity. The AGN fractional luminosity as a function of total IR luminosity has been studied since *IRAS* galaxies were discovered. Optical spectroscopy (Veilleux et al. 1995) found that the fraction of *IRAS* sources with AGN spectra, and the fraction of Seyfert galaxies amongst the AGN increases with increasing IR luminosity, reaching values of 62 and 54 per cent, respectively, at IR luminosities $>10^{12}$ $L_{\odot}$. Near-IR spectroscopy of

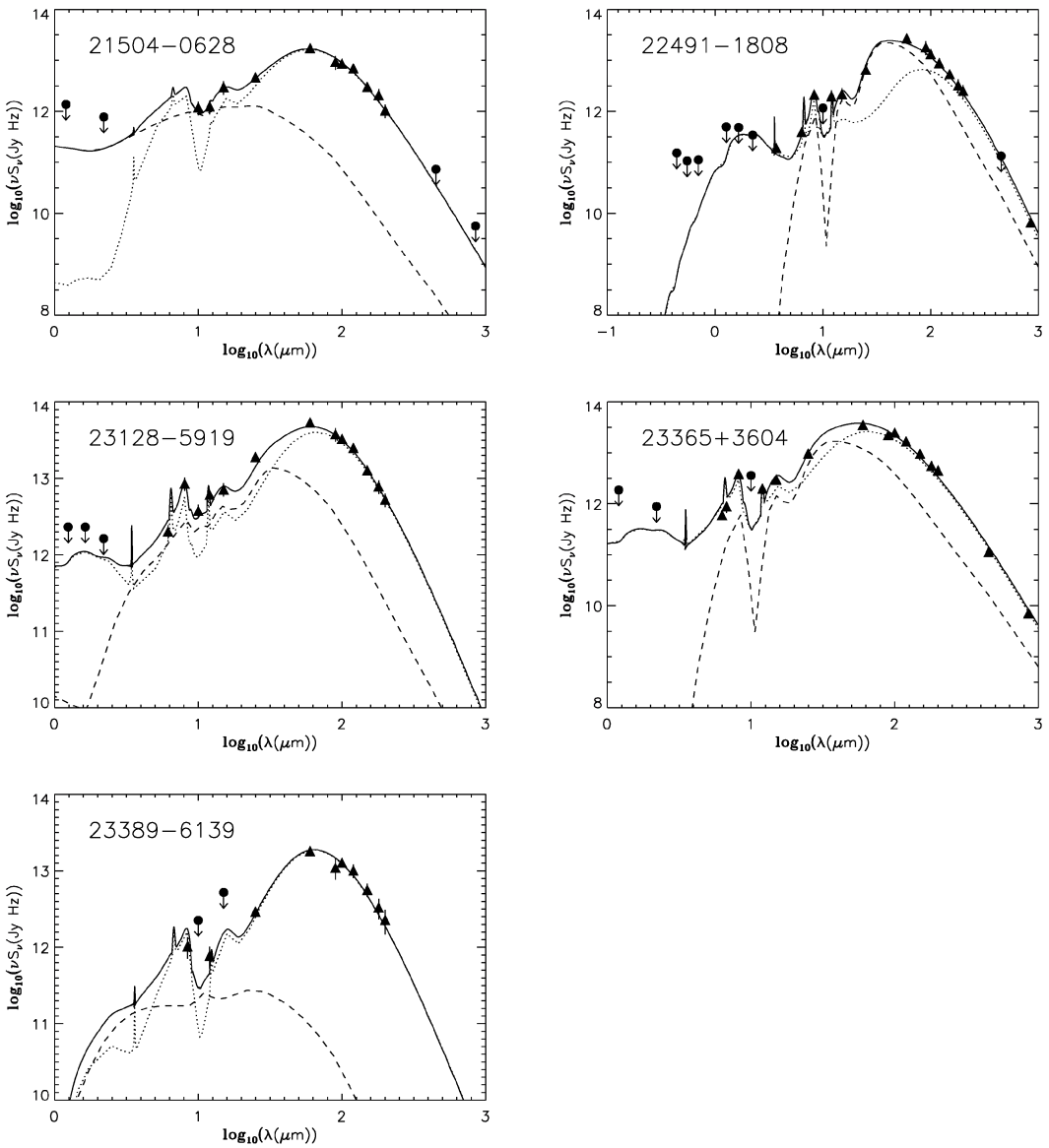

Figure 1 – *continued*

ULIRGs (Veilleux et al. 1999) shows that the fraction of ULIRGs with signs of AGN activity is at least 20–25 per cent, but rises abruptly to 35–50 per cent for objects with $L_{\rm IR} > 10^{12.3}$ $L_{\odot}$. Recent *ISO* spectroscopy of a small sample of ULIRGs (Tran et al. 2001) found half of the sample to be starburst-dominated and half to be AGN dominated. They also showed that, at IR luminosities below $10^{12.4}$ $L_{\odot}$, most ULIRGs were starburst dominated, with the starburst contributing around 85 per cent to the IR emission. At IR luminosities above $10^{12.4}$ $L_{\odot}$ the AGN contribution was much higher, with the starburst contributing approximately 50 per cent of the IR emission on average. Starburst dominated systems were found up to luminosities of around $10^{12.65}$ $L_{\odot}$.

From our results, we find that both starburst and AGN activity are central in understanding the properties of local ULIRGs. All 41 objects in our sample contain a very luminous starburst that contributes significantly (at least 28 per cent) to the total IR luminosity. There are no purely AGN-powered systems in the sample. 23/41 objects have measured AGN luminosities where the AGN contributes significantly to the total IR emission, the remaining 18 objects have only upper limits on the AGN contribution. In three cases the AGN supplies more than half of the total IR emission, in the remaining cases the starburst is the dominant contributor. We therefore find that previous estimates of the fraction of local ULIRGs that are starburst dominated based on mid-IR spectroscopy have underestimated the true fraction, and that this fraction is ∼90 per cent rather than 80 per cent. The mean starburst fractional luminosity for the sample is 82 per cent, spanning the range 28 to ∼100 per cent. Overall, the IR emission from ULIRGs as a class is either starburst in origin with a negligible AGN contribution, or arises from a combination of starburst and AGN activity with the starburst usually contributing the largest fraction. Given our sample size, the fraction of purely AGN-powered local ULIRGs must be less than ∼2 per cent. The derived star formation rates range from 50 to 500 $M_{\odot}$ yr^{-1} and the derived dust masses span the range $10^7 < M_{\odot} < 10^9$. These ranges

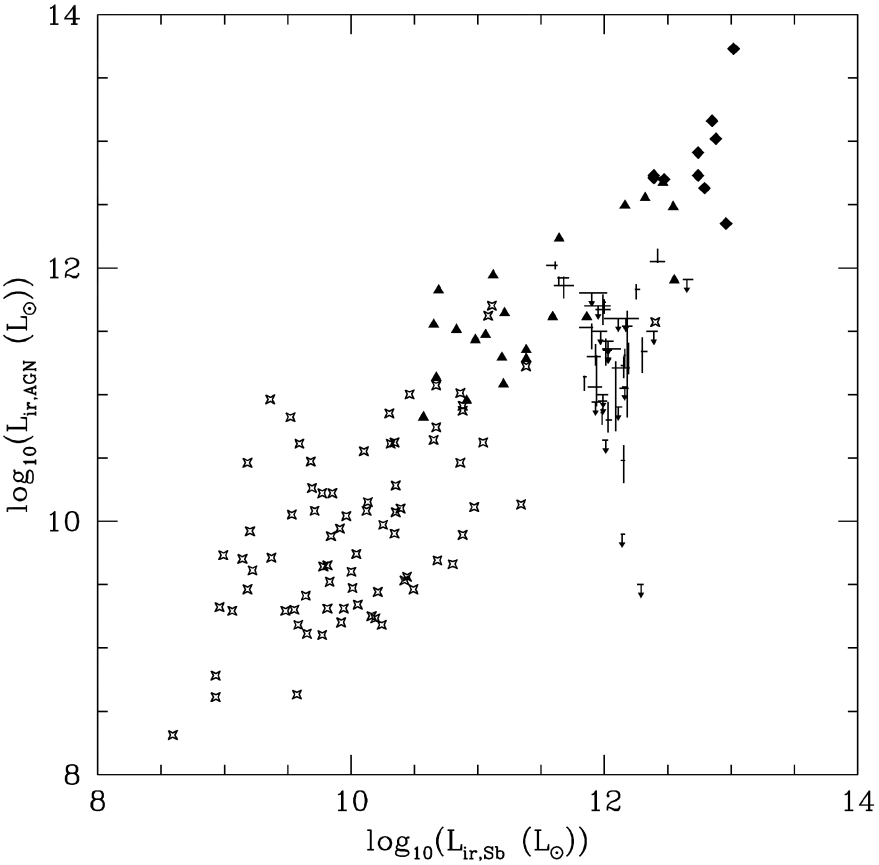

Figure 2. AGN luminosity in the IR plotted against starburst luminosity in the IR. The ULIRGs from our sample are plotted as points, with a downward arrow indicating an upper limit on the AGN luminosity. Triangles are PG QSOs, and crosses are those galaxies with detections in all four *IRAS* bands, both these samples are taken from Rowan-Robinson (2000). Diamonds are the hyperluminous infrared galaxies taken from Farrah et al. (2002b).

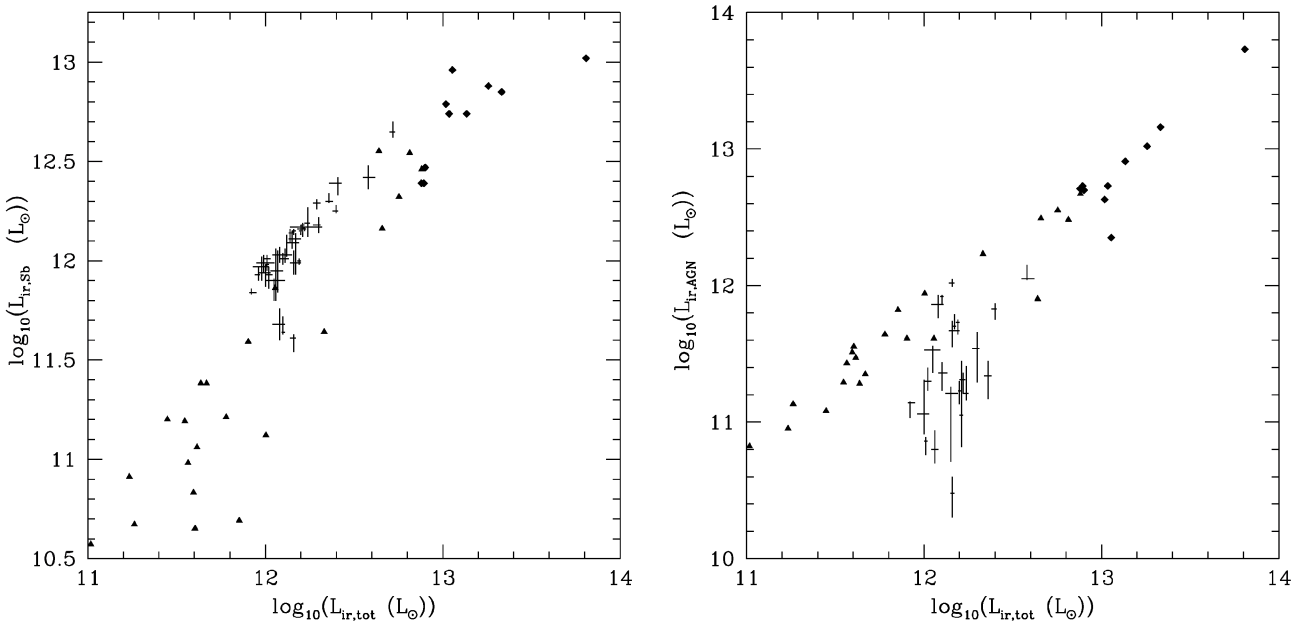

Figure 3. Total IR luminosity plotted against (left) starburst luminosity and (right) AGN luminosity. Our ULIRGs are plotted as points, triangles are PG QSOs taken from Rowan-Robinson (2000) and diamonds are the HLIRGs from Farrah et al. (2002b).

are at least one order of magnitude higher than those observed in normal galaxies, indicating that all ULIRGs are going through a major star-forming episode. It proved difficult to constrain the line of sight to the AGN torus, with meaningful constraints only achieved for a few objects. Although these values are discussed in Section 5 we cannot draw any general conclusions concerning relative AGN orientation in ULIRGs.

Fig. 2 shows a plot of starburst luminosity versus AGN luminosity. Also plotted are the starburst and AGN luminosities of 10 hyperluminous infrared galaxies (HLIRGs, diamonds) taken from Farrah et al. (2002b), as well as 22 PG QSOs (triangles) and 78 galaxies with detections in all four *IRAS* bands (crosses). The two latter samples are taken from Rowan-Robinson (2000) and rescaled to $H_0 = 65\,\mathrm{km\,s^{-1}\,Mpc^{-1}}$. The figure shows that starburst and AGN luminosities are correlated, albeit with a large scatter, over six orders of magnitude in IR luminosity and over a wide range of galaxy types. Therefore, there may be a common physical factor governing the IR luminosity of both starbursts and AGN in these galaxies. We postulate that this factor is the available quantities of gas and dust in the nuclear regions of these systems, as this affects both the rate and duration of black hole accretion, and the number of stars that can form.

Next, we examine trends in starburst and AGN luminosity against total IR luminosity. Fig. 3 shows total IR luminosity plotted against starburst luminosity and AGN luminosity. Also plotted are the PG QSO and HLIRG samples, however, in this section we only discuss the ULIRGs plotted in these figures; comparisons between the ULIRGs, PG QSOs and HLIRGs can be found in Section 6.4.2. The left-hand panel shows that the ULIRG starburst luminosity is strongly correlated with the total luminosity. From the right-hand plot in Fig. 3 we can see that, although there is a trend for more luminous ULIRGs to contain a more luminous AGN, the trend is less clear than for the starburst luminosity. Fig. 4 shows total IR luminosity plotted against *fractional* AGN luminosity. It can be seen that there is no trend for increasing AGN dominance with increasing total luminosity in ULIRGs, contrary to previous claims.

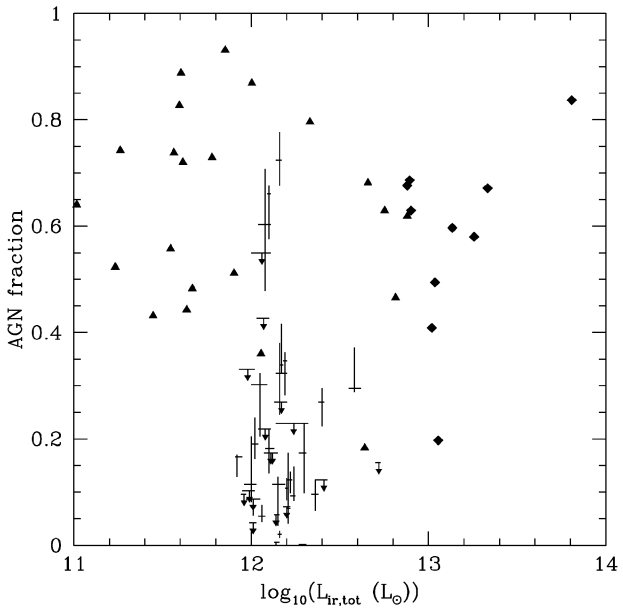

Figure 4. Total luminosity in the IR plotted against the AGN fraction. The key to the symbols is the same as for Fig. 3.

We find that these claims were based on finding generally more luminous AGN in more luminous ULIRGs, but that there is no evolution of fractional AGN luminosity with total luminosity in local ULIRGs.

6.2.2 *Multiple starbursts and multiple mergers*

The number of individual starburst events that occur over the lifetime of a ULIRG is an important parameter in understanding starburst triggering and evolution in all classes of active galaxy. Similarly, the number of progenitors in a typical ULIRG merger can be used to estimate what fraction of ULIRGs occur in the field galaxy population between two or three progenitors, and what fraction occurs in compact groups of galaxies between multiple progenitors.

Both of these parameters have proved difficult to estimate. Numerical simulations of mergers between two galaxies have shown that multiple, discrete starburst events can be triggered even in double mergers. The timing of the starbursts is thought to depend on the progenitor galaxy morphologies, with early starbursts (before the galaxies start to merge) occurring in bulgeless disc galaxies, and late starbursts (after the galaxies have started to merge) occurring in disc galaxies with a bulge component (Mihos & Hernquist 1994, 1996). Simulations of multiple galaxy mergers have, however, shown that more than two starburst or AGN nuclei is evidence that there were more than two merger progenitors (Taniguchi & Shioya 1998), and that repetitive starbursts are characteristic of multiple mergers (Bekki 2001). Observationally, multiple mergers have been linked to Arp 220 (Diamond et al. 1989) and to larger samples of ULIRGs (Borne et al. 2000; Farrah et al. 2001). Other authors have estimated the lifetime of a single starburst event in ULIRGs. Thornley et al. (2000) derive a starburst lifetime range of 10^6–10^7 yr, and infer that galactic superwinds produced by supernovae may be responsible for the short duration. Genzel et al. (1998) derive an upper limit on the starburst lifetime in ULIRGs of $\sim 10^8$ yr. The lifetime of a ULIRG has been previously estimated to lie in the range 10^8–10^9 yr (Farrah et al. 2001; Murphy et al. 2001) based on the observed range of morphologies in large samples of ULIRGs, the apparent discrepancy between the ULIRG and starburst lifetimes has led to the suggestion that multiple starbursts and multiple mergers may be common in ULIRGs (Farrah et al. 2001).

The starburst ages derived for our sample are listed in Table 4. As our sample is large and the selection is robust we are confident that this range in ages is representative of the ULIRG population as a whole. Excluding those objects with upper or lower limits on the starburst age, the derived ages span the range $1.6 \times 10^6 \leqslant \mathrm{yr} \leqslant 7.1 \times 10^7$, with most lying in the range $1.0 \times 10^7 \leqslant \mathrm{yr} \leqslant 3.7 \times 10^7$. These lifetime ranges are clearly inconsistent with a single starburst event powering the IR emission for the lifetime of a ULIRG. From Section 6.2.1, however, starbursts are present in at least 98 per cent of ULIRGs and in most cases dominate the IR emission; AGN activity cannot therefore explain this discrepancy in lifetimes. We therefore find that multiple starburst events must be common in the ULIRG population, and by inference that multiple mergers must be common as well.

From this analysis, coeval starbursts with different ages are feasible in ULIRGs, and it is important to note the effects this may have on our SED fitting approach. Whilst the available photometry is sufficient to separate starburst and AGN emission, it is not sufficient to resolve the starburst emission into multiple components. The derived age ranges in Table 4 should, however, encompass the age ranges of any coeval starbursts, due to the effect of age on the

shape of the starburst SED. As the age of the starburst increases then (with reference to fig. 3 of Efstathiou et al. 2000), the peak of the SED shifts to longer wavelengths, PAH features become stronger, the 9.8-μm silicate absorption feature becomes shallower, and the optical/UV flux increases. Hence, the mid- and far-IR photometry, in constraining the strength of the mid-IR spectral features and the peak of the SED, respectively, provide a lower limit to ages of any coeval starbursts, whereas the optical photometry provides an upper limit. Therefore, even if some or all of the ULIRGs in our sample contained two or more starbursts with different ages, we are confident that the starburst age ranges given in Table 4 encompass the ages of these starbursts.

6.3 Observational diagnostics of ULIRGs

6.3.1 Mid-infrared spectroscopy

Several groups have constructed diagnostics for the power source in ULIRGs based on mid-IR spectra from *ISO* observations, specifically using the relative strengths of the unidentified infrared emission band (UIB) features lying between 5 and 12 μm. Currently, the most prevalent of these diagnostics is that proposed by Genzel et al. (1998). In this diagnostic the ratio of the 7.7-μm emission, thought to arise from PAHs, relative to the continuum emission at the same wavelength is used to differentiate between starburst and AGN emission. A high value of $F_{7.7}/C_{7.7}$ (>1) indicates starburst power, whereas a lower value of $F_{7.7}/C_{7.7}$ indicates AGN power. This is generally borne out by mid-IR observations of lower-luminosity starburst and AGN systems (e.g. Rigopoulou et al. 1999). There are, however, potential problems with this approach. First, since the active regions in ULIRGs are small and dusty it is not clear that even mid-IR observations can penetrate to the central regions, although it is argued that this is unlikely to be significant (Genzel et al. 1998; Rigopoulou et al. 1999; Tran et al. 2001). Secondly, some metal-poor dwarf starburst galaxies show no UIB features, but as ULIRGs are not metal-poor this is also argued not to be important (Rigopoulou et al. 1999).

By comparing the results from diagnostics using the $F_{7.7}/C_{7.7}$ ratio to our results for the 22 ULIRGs common to our sample and to Rigopoulou et al. (1999), we can examine the reliability of the $F_{7.7}/C_{7.7}$ technique. In Fig. 5 we plot $F_{7.7}/C_{7.7}$ against starburst luminosity and fractional AGN luminosity. From the left-hand plot it can be seen there is, at best, a weak trend for more luminous starbursts to have *lower* values of $F_{7.7}/C_{7.7}$. The immediate possibility is that the mid-IR diagnostics are correct and our SED fitting approach is wrong, however, our SED fits reproduce the observed $F_{7.7}/C_{7.7}$ ratios in all 22 objects, and the observed SED from the near-UV to the submillimetre. We therefore infer that, of the two approaches, ours is more robust. Therefore, it seems that the relative strength of the 7.7-μm PAH feature is not a reliable indicator of the luminosity of the starburst, but merely of its presence. We postulate that the discrepancy between the nature of the 7.7-μm PAH feature in ULIRGs and in less luminous starburst galaxies is due to two reasons. First, in ULIRGs it is more likely than in moderate starbursts that the obscuration is so high that spectral features are not apparent in the mid-IR. Secondly, the intense UV radiation in ULIRG-like starbursts may be capable of dissociating the hydrocarbon bonds in PAHs. Both of these reasons would explain why more luminous starbursts have smaller $F_{7.7}/C_{7.7}$ ratios.

More serious, however, is that the right-hand panel of Fig. 5 shows no correlation between $F_{7.7}/C_{7.7}$ and the fractional AGN luminosity, from which we infer that the $F_{7.7}/C_{7.7}$ ratio *on its own* is not an accurate indicator of the overall power source in ULIRGs. This discrepancy between our results and those of Rigopoulou et al. (1999) can also be explained by the more extreme nature of ULIRGs. From our results, all ULIRGs contain a starburst, explaining the prevalence of PAH features in their mid-IR spectra, however, the majority of ULIRGs are composite systems and may contain a heavily obscured starburst or AGN that does not emit significantly in the mid-IR but that does emit strongly in the far-IR/submillimetre. As an

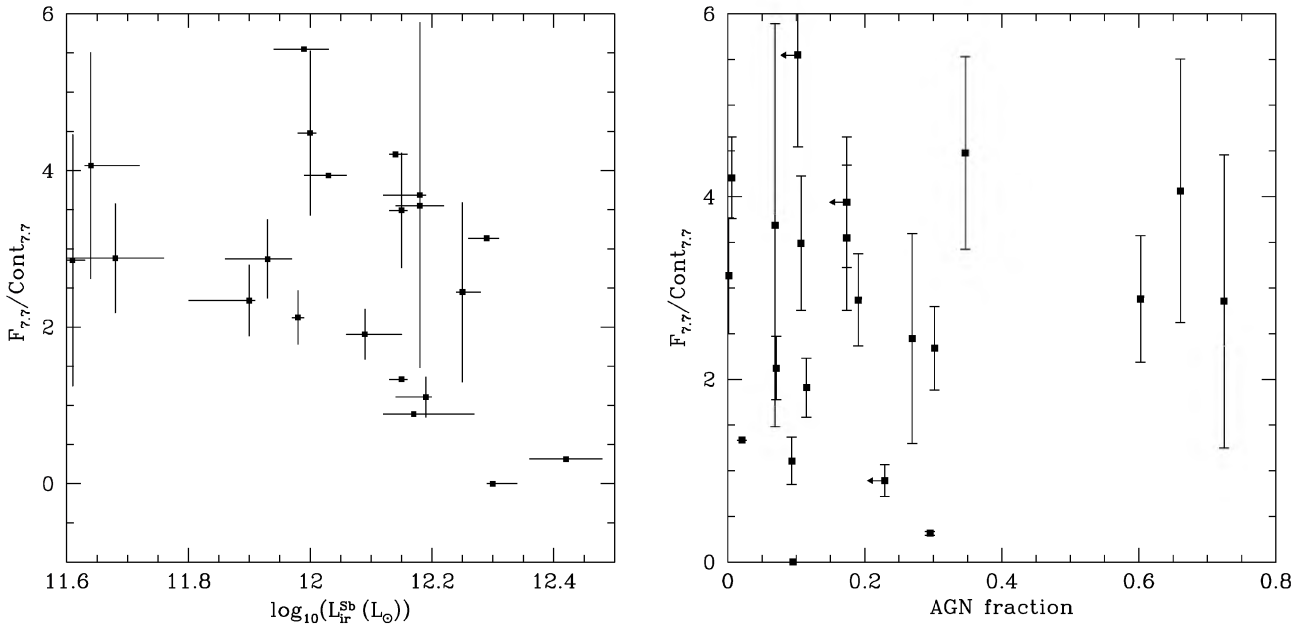

Figure 5. Left: starburst luminosity plotted against the 7.7-μm line/continuum ratio from Rigopoulou et al. (1999). Right: fractional AGN luminosity plotted against the 7.7-μm line/continuum ratio.

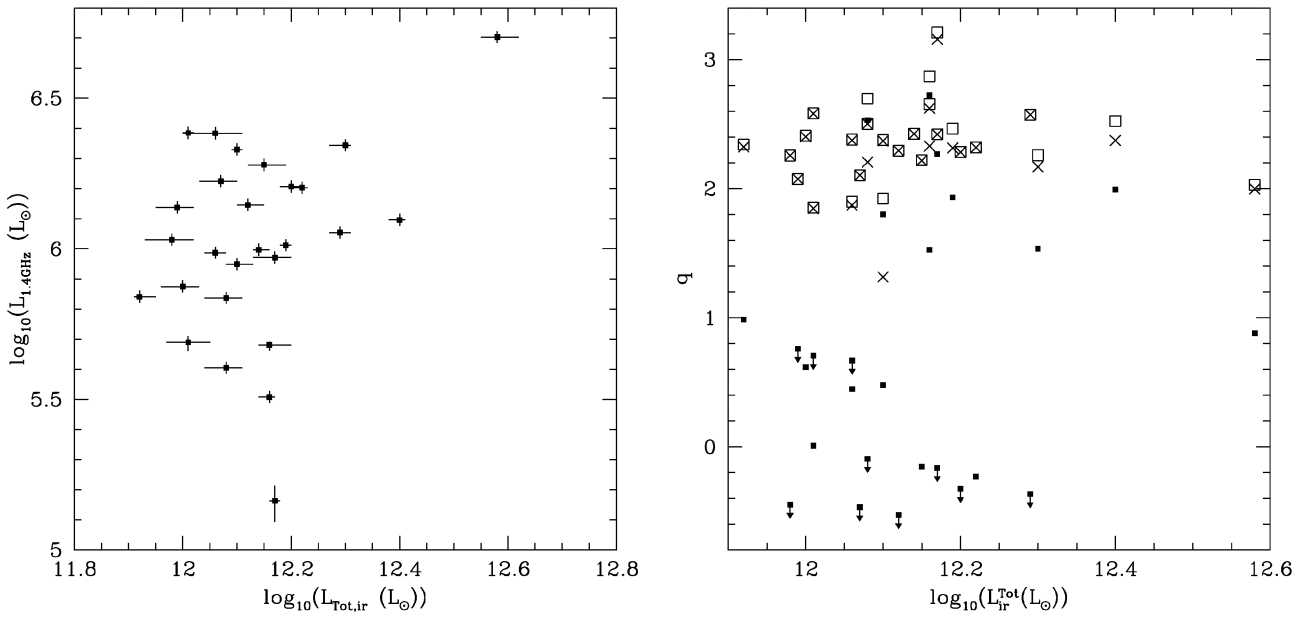

Figure 6. Left: total IR luminosity plotted against the total radio luminosity. Right: total IR luminosity versus the q parameter. Open squares are $q_{\rm total}$, crosses are $q_{\rm starburst}$, and small filled squares are $q_{\rm AGN}$. A downward arrow indicates an upper limit.

example we consider IRAS 00262+4251. This object, with $F_{7.7}/C_{7.7} = 4.063$ is classified as a pure starburst by Rigopoulou et al. (1999). From our SED fit, however, (Fig. 1), the AGN does not contribute in the mid-IR as the torus is viewed almost edge on and the corresponding obscuration in the mid-IR is very high. At wavelengths between 50 and ~120 μm the AGN contribution is, however, dominant. Although this object does contain a starburst, overall the emission is mainly due to AGN activity. We conclude that the $F_{7.7}/C_{7.7}$ ratio on its own is only an indicator of whether a ULIRG contains a moderately obscured and moderately luminous starburst. It cannot be used to probe either heavily obscured or very luminous starburst activity, or AGN that are either isotropically obscured or oriented nearly edge on relative to us. As such, it cannot be used on its own to probe the overall power source in ULIRGs.

6.3.2 The radio-infrared correlation

There is observed to exist a tight correlation between radio and infrared flux for both normal and active galaxies, extending over several orders of magnitude (Helou, Soifer & Rowan-Robinson 1985). The physical origin of this relation is believed to be a population of relativistic electrons accelerated by supernova remnants produced in regions of massive star formation (Harwit & Pacini 1975). This relation is usually expressed using the parameter q, the logarithm of the ratio of infrared flux to radio flux. For starburst galaxies and ULIRGs, q is observed to lie in the range $2.0 < q < 2.6$ (Condon et al. 1991). Radio-loud quasars, on the other hand, have typical q values in the range $0 < q < 1$ (e.g. Roy et al. 1998), whereas radio-quiet quasars have q values lying in a similar range to local starburst galaxies and ULIRGs (Sopp & Alexander 1991). It has therefore been suggested that the radio–IR correlation in both ULIRGs and radio-quiet quasars is due to star formation (Condon et al. 1991; Cram, North & Savage 1992).

Using the results from this paper we can examine the origin of the radio–IR correlation for ULIRGs, and the factors that may bias it. 1.4-GHz fluxes were obtained for most of the objects in our sample from the NVSS catalogues, these fluxes are presented in Table 5. The left-hand panel of Fig. 6 shows total IR luminosity plotted against 1.4-GHz luminosity, and a weak, though positive, correlation can be seen. Fig. 7 shows the starburst and AGN luminosities plotted against 1.4-GHz luminosity. The correlation between the radio luminosity and the starburst luminosity is stronger than for the total luminosity, whereas no correlation is observed with the AGN luminosity. We thus confirm that the radio–IR correlation in ULIRGs is due to star formation.

We have further investigated this relation using the q parameter. To allow future comparisons with galaxy samples that do not benefit from accurate estimates of IR luminosities from SED fits, we express q as

$$q = \log\left(\frac{F_{60}}{F_{1.4}}\right), \tag{5}$$

where $F_{1.4}$ is the 1.4-GHz flux and F_{60} is the rest-frame 60-μm flux. Rest-frame 60-μm fluxes were extracted from the best-fitting total, starburst and AGN SEDs. In Table 5 we present values of q calculated using these fluxes. We derive $\langle q_{\rm total}\rangle = 2.36 \pm 0.06$, $\langle q_{\rm starburst}\rangle = 2.29 \pm 0.06$ and $\langle q_{\rm AGN}\rangle = 1.29 \pm 0.25$, which are in agreement with previous estimates for ULIRGs. Individual q values are plotted against total IR luminosity in the right-hand panel of Fig. 6. It is evident that $q_{\rm total}$ and $q_{\rm starburst}$ have only a small scatter about a mean value, but that the values of $q_{\rm AGN}$ appear randomly distributed.

If the radio–IR correlation in ULIRGs is due to star formation, then what is the origin of the scatter about the mean values of $q_{\rm starburst}$ and $q_{\rm total}$? Broadly, there are four possibilities. First, the IMF of the starburst may be skewed towards or away from producing high-mass stars, thus producing an over- or underabundance of radio supernova remnants, thus causing a scatter. This possibility is impossible to investigate within the context of this paper. Secondly, there may be contamination of the 1.4-GHz luminosity from an obscured AGN, leading to an artificially suppressed q value. We argue that this possibility, although undoubtedly present in the ULIRG population, is

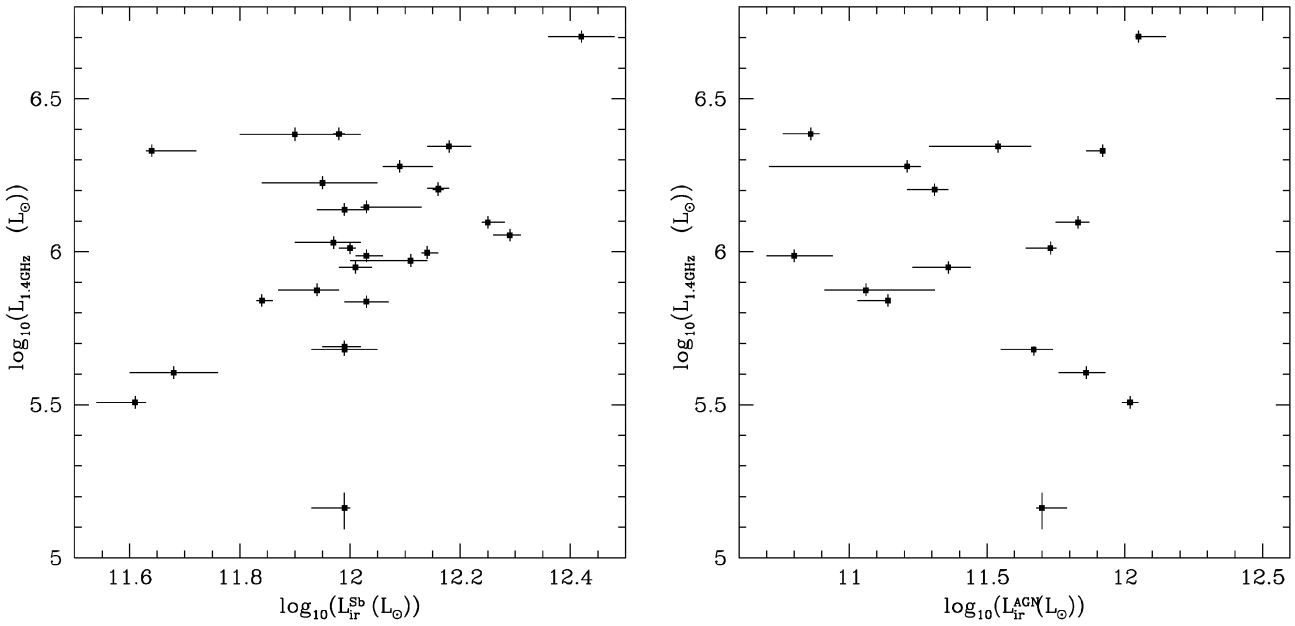

Figure 7. Left: starburst luminosity plotted against 1.4-GHz radio luminosity. Right: AGN luminosity plotted against 1.4-GHz radio luminosity.

Table 5. Ultraluminous infrared galaxies detected in the radio band.

Name	$F_{1.4\,\mathrm{GHz}}$	q_{total}	$q_{\mathrm{starburst}}$	q_{AGN}
00262+4251	28.0	1.92	1.32	1.80
00335−2732	11.25	2.60	2.58	<0.70
04232+1436	29.39	2.10	2.10	< −0.4
05189−2524	28.8	2.66	2.62	1.53
08572+3915	4.3	3.21	3.16	2.27
09320+6134	170.1	1.85	1.85	0.00
09583+4714	36.5	1.90	1.87	<0.60
10035+4852	28.1	2.26	2.26	< −0.40
10494+4424	21.2	2.28	2.28	< −0.30
10190+1322	16.8	2.38	2.37	0.48
10565+2448	56.9	2.38	2.37	0.45
12112+0305	23.3	2.57	2.57	< −0.37
12540+5708	308	2.03	2.00	0.88
13428+5608	144	2.22	2.22	−0.15
14348−1447	35.8	2.26	2.17	1.53
14378−3651	33.8	2.29	2.29	< −0.50
15250+3609	14.5	2.70	2.21	2.53
15327+2340	326.5	2.42	2.42	< −1.0
17132+5313	29.3	2.34	2.32	0.98
17208−0014	81.8	2.07	2.07	<0.76
18470+3233	12.4	2.50	2.50	< −0.08
19458+0944	14.0	2.52	2.37	1.99
20046−0623	14.6	2.42	2.42	< −0.16
20414−1651	23.4	2.32	2.32	−0.23
21504−0628	13.8	2.41	2.40	0.62
22491−1808	5.9	2.87	2.33	2.72
23365+3604	27.2	2.47	2.31	1.93

1.4-GHz radio fluxes were taken from the NVSS catalogues and are in mJy. The q values were calculated using equation (5).

not the main cause of the observed scatter. If there were a significant number of obscured AGN causing the scatter, then we would expect to see some correlation between AGN luminosity and radio luminosity, and yet none is observed. Even if only the most IR-luminous AGN are plotted in Fig. 6, no such correlation appears. The third possibility is that the starburst may be too young to have formed a significant population of radio supernova remnants, thus causing an artificial amplification of the q parameter. We argue that this is a negligible effect in the ULIRG population for two reasons. First, most of the starburst ages lie in the range 10–37 Myr, by which time a significant population of supernova remnants will certainly have formed. Secondly, if the youngest starbursts are removed from the left-hand plot of Fig. 7 then the scatter becomes bigger rather than smaller. The fourth possibility is an old relativistic electron population from a previous starburst event. As described in Section 6.2.2 it is likely that ULIRGs undergo multiple, discrete starburst events with lifetimes in the range 10^6–10^8 yr. Although radio supernova remnants have lifetimes of only 10^3 yr at best, the relativistic electrons they produce have lifetimes of the order of 10^8 yr (Condon 1992). This lifetime lies at the upper end of the lifetime range of a single starburst event, and is comparable to the total lifetime of a ULIRG. We thus conclude that most of the scatter around the radio–IR correlation for ULIRGs is due to skewed IMFs in the starburst, and relativistic electrons from a previous, separate starburst event.

6.4 ULIRG evolution

6.4.1 Do ULIRGs evolve into QSOs?

The first picture of ULIRG evolution to be proposed was that of Sanders et al. (1988), which asserted that ULIRGs as a class evolve into optical QSOs. According to this picture (hereafter referred to as the S88 picture), interactions and mergers between gas-rich spirals transport gas to the central regions of the galaxies. This central gas concentration fuels starburst activity, and in the latter stages of the merger commences the fuelling of a central supermassive black hole, which rapidly comes to dominate the IR luminosity of the ULIRG. In the final stages the dust shrouding the black hole is blown away and the ULIRG evolves into an optical QSO. A qualitatively similar picture was also proposed by Canalizo & Stockton (2001).

A more recent evolutionary scenario for ULIRGs is that of Farrah et al. (2001), also later suggested by Tacconi et al. (2002). In this scenario ULIRGs are not simply the dust-shrouded precursors to optical QSOs but instead are a diverse population with a broad range of properties and evolutionary paths. Although some ULIRGs would still evolve into QSOs, this number would be a small and non-representative subset of the ULIRG population.

Previous studies of the evolution of ULIRGs have highlighted some problems for the S88 picture. In the mid-IR, spectroscopic studies of ULIRGs (Genzel et al. 1998; Rigopoulou et al. 1999) find no evidence that the advanced merger systems are more AGN-like, based on the ULIRG nuclear separations. That AGN activity becomes more prevalent with merger advancement is a natural prediction of the S88 picture. Furthermore, a recent spectroscopic study of the stellar and gas kinematics in ULIRGs (Genzel et al. 2001) found that ULIRGs will likely evolve into only $\sim L_*$ ellipticals, and not into the most massive ellipticals seen locally. A corollary to this are the results from a large-scale imaging and spectroscopy survey of ULIRGs (Veilleux, Kim & Sanders 2002), in which it was found that nearly half the sample may not evolve into an optical, post-ULIRG AGN, and that merger-induced QSO activity might only take place if both merger progenitors had L_* luminosities or greater.

Using the results from this paper, and from previous authors, we can examine these two evolutionary scenarios. We first consider the growth of supermassive black holes (SMBHs) in ULIRG mergers, and relate this to the SMBH masses seen in QSOs, and to the level of AGN activity seen in our sample. Nearly all optical QSOs with measured SMBH masses have $M_{\rm BH} \geqslant 10^8$ M$_\odot$, in some cases reaching $M_{\rm BH} \sim 10^{10}$ M$_\odot$ (Gu, Cao & Jiang 2001; McLure & Dunlop 2001), hence it seems likely that an SMBH in this mass range is necessary for QSO activity. The growth of SMBHs in ULIRG mergers has been studied by Taniguchi, Ikeuchi & Shioya (1999). They conclude that an SMBH of mass $\sim 10^8$ M$_\odot$ can form if any of the progenitor galaxies contains a 'seed' SMBH of mass $\geqslant 10^7$ M$_\odot$ undergoing efficient Bondi-type gas accretion over $\sim 10^8$ yr.

Hence, if the S88 picture is correct and ULIRGs as a class evolve into QSOs, then the range of SMBH masses seen in spiral galaxies [$10^6 < M_{\rm BH}(\rm M_\odot) < 10^8$] would have to be transformed by the merger into the SMBH mass range seen in QSOs [$10^8 < M_{\rm BH}(\rm M_\odot) < 10^{10}$]. This would require very efficient accretion on to the black hole for the entire duration of the merger. This itself implies that the lifetime of the IR-luminous AGN phase will be significantly greater than the lifetime of any single starburst event. Furthermore, in order to achieve the SMBH mass range seen in QSOs, then the AGN in a ULIRG observed at a random point during the merger would in many cases harbour an SMBH of mass $M_{\rm BH} \geqslant 10^8$ M$_\odot$. Overall therefore, if the S88 picture is correct, then most ULIRGs should contain a long-lived AGN which, by virtue of efficient accretion on to an SMBH with mass comparable to those seen in QSOs, should have an IR luminosity comparable to the bolometric luminosity seen in QSOs. Our results, however, do not support this, as we find all ULIRGs to contain a very luminous starburst, with only approximately half containing a luminous AGN, and that less than 10 per cent of ULIRGs are AGN dominated. Whilst we cannot rule out the S88 picture based on AGN activity alone, it seems unlikely that the level of AGN activity seen in our sample could transform the BH mass range in spirals into that seen in QSOs.

Next, we consider the nature of the so-called 'warm' ULIRGs, those with $F_{25}/F_{60} > 0.25$ (where F_{25} and F_{60} are the *IRAS* 25- and 60-μm fluxes, respectively). Objects with 'warm' infrared colours have been previously shown to be more likely to contain IR-luminous AGN. Hence, if the S88 picture is true, then the greater prevalence of AGN in 'warm' ULIRGs than in cool ones means that 'warm' ULIRGs will be, on average, nearer the end of the ULIRG phase than 'cool' ULIRGs, and closer to evolving into optical QSOs. Therefore, 'warm' ULIRGs should have a higher *fractional* AGN luminosity on average than 'cool' ULIRGs as the AGN comes to dominate the bolometric emission and the starburst dies away. Fig. 8 shows the F_{25}/F_{60} colour plotted against AGN luminosity and fractional AGN luminosity for the objects in our sample. Values of F_{25}/F_{60} are presented in Table 1. As expected, those objects with a higher value of F_{25}/F_{60} are more likely to contain a more luminous AGN. There is, however, no trend of increasing AGN fractional luminosity with increasing IR colour.

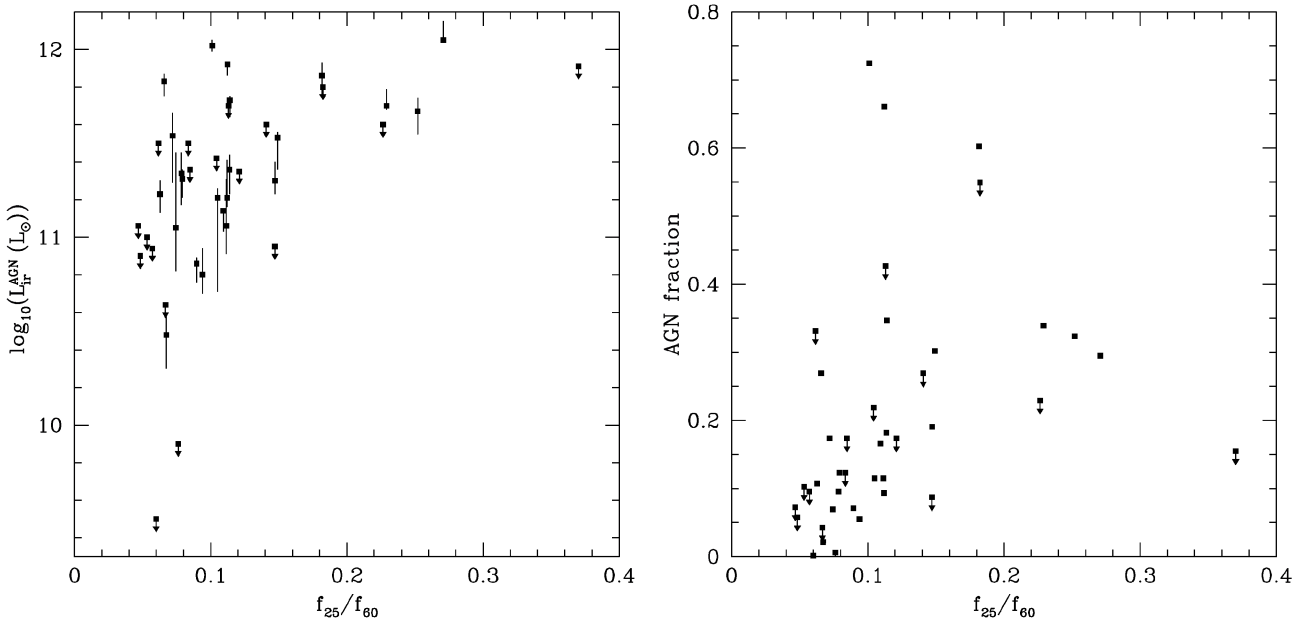

Figure 8. F_{25}/F_{60} colour plotted against (left) AGN luminosity and (right) fractional AGN luminosity.

Overall therefore, our results contradict the S88 picture, and imply that ULIRGs as a class do not evolve to become QSOs. Instead, the wide range of starburst and AGN luminosities derived for our sample imply multiple possible patterns of starburst and AGN activity over the lifetime of the ULIRG, in line with the Farrah et al. (2001) picture. The overall level of AGN activity is consistent with sufficient accretion to transform the range of black hole masses seen in spirals into the range of black hole masses seen in ellipticals, without recourse to an optical QSO phase. As a small number of our sample are AGN-dominated it is likely that some ULIRGs do become optical QSOs, but the small number of such systems in our sample argues that such ULIRGs are rare, and thus unrepresentative of the ULIRG population as a whole.

6.4.2 ULIRG evolution with redshift

ULIRGs, despite being rare in the local Universe, are a cosmologically important galaxy population. At low redshifts the ULIRG luminosity function shows strong evolution with redshift (Veilleux et al. 1999). In addition, deep submillimetre surveys find that systems with ULIRG-like luminosities dominate the global energy density of the Universe at $z \geqslant 1$ (Barger et al. 1998; Lilly et al. 1999; Fox et al. 2002; Scott et al. 2002). Determining how systems with ULIRG-like luminosities evolve with redshift is therefore necessary to measure, for example, the overall star formation history of the Universe, currently a hotly debated topic (e.g. Madau et al. 1996; Rowan-Robinson et al. 1997).

It is, however, not known whether the IR luminosity of these high-redshift sources arises due to mergers between two or more large spiral galaxies, as in local ULIRGs, or via a different mechanism. If the former is true then the strong evolution seen in the ULIRG luminosity function will most likely be due to mergers between two or more large spiral galaxies becoming more common with increasing redshift. If the latter is true then this indicates that the strong evolution seen in the ULIRG luminosity function is probably due to different galaxy formation processes becoming more important at high redshifts. Currently, the only sample of IR luminous sources at high redshift with resolved starburst and AGN components is the sample of HLIRGs presented by Farrah et al. (2002b). On morphological grounds there is some evidence that the trigger for the IR emission in local ULIRGs and high-z HLIRGs is the same; nearly all ULIRGs show signs of morphological disturbance (Borne et al. 2000; Farrah et al. 2001), as do approximately half of HLIRGs (Farrah et al. 2002a).

In Section 6.2.1 we showed that the broad correlation between starburst and AGN luminosities for a wide range of galaxy types, including ULIRGs and HLIRGs, was most plausibly explained by the starburst and AGN luminosities being governed by the gas and dust masses in the nuclear regions. We now examine whether the *evolution* of the starburst and AGN components are the same or different between ULIRGs and HLIRGs, to determine whether HLIRGs are the high-redshift analogues of ULIRGs or a different galaxy population, by comparing the ULIRGs from our study with the HLIRGs from Farrah et al. (2002b). Both samples span a similar range in fractional AGN luminosity, ranging from almost pure starbursts to AGN-dominated systems. Amongst the ULIRGs most systems are starburst dominated with a mean starburst fraction of 82 per cent, whereas in the HLIRG population approximately half the systems are AGN dominated, with a mean starburst fractional luminosity of ~35 per cent. This difference could be because a more luminous AGN is required to generate the higher total luminosities in HLIRGs, however, starburst dominated HLIRGs are found amongst the most luminous members of the HLIRG population. This then constitutes a distinct difference between the two samples. Amongst local ULIRGs, starbursts are the dominant contributor to the total luminosity, whereas amongst HLIRGs, although a starburst could, in principle, accomplish the same thing, this is not observed and AGN activity is much more prevalent than in ULIRGs. This can also be seen in Figs 3 and 4, in which the starburst and AGN luminosities are compared with the total IR luminosities in ULIRGs, HLIRGs and PG QSOs. Furthermore, it can also be seen from these figures, particularly the right-hand panel of Fig. 3, that the pattern of starburst and AGN activity in HLIRGs is much more reminiscent of the pattern seen in QSOs than in ULIRGs.

Based on this comparison, we conclude that IR-luminous galaxies at $z \sim 0$ and $z \geqslant 1$ are physically different galaxy populations. We speculate that this difference is due to different galaxy formation processes in the low- and high-redshift Universe, and that the trigger for starburst and AGN activity in high-redshift IR-luminous sources is more similar to the trigger for QSO activity, rather than the trigger for ULIRG activity in the local Universe. At low z, ULIRGs are formed via the merger of two or more gas-rich spiral galaxies. At high redshift, however, the galaxy formation processes were probably more diverse, with hierarchical buildup from many small dwarf galaxies or monolithic collapse of a large disc of gas forming a primeval galaxy both being leading possibilities.

7 CONCLUSIONS

We have studied the properties of a sample of 41 local Ultraluminous Infrared Galaxies using archival optical and infrared photometry and advanced radiative transfer models for starbursts and AGN. Our conclusions are as follows.

(i) All of the sample contain a luminous starburst, whereas approximately half contain a luminous AGN. The mean starburst fractional luminosity is 82 per cent, and in ~90 per cent of the sample the starburst produces more than half the total IR emission. We conclude that the fraction of purely AGN-powered ULIRGs in the local Universe is less than 2 per cent. By combining our objects with other galaxy samples we find that starburst and AGN luminosities correlate over six orders of magnitude in total IR luminosity and over a wide range of galaxy types, suggesting that a common physical factor, most plausibly the gas masses in the nuclear regions, govern both the starburst and AGN luminosities.

(ii) The starburst luminosity shows a strong positive correlation with total luminosity, as does the AGN luminosity, albeit less strongly. We, however, find no trend for increasing fractional AGN luminosity with increasing total luminosity, contrary to previous claims. We find that these claims were based on finding generally more luminous AGN in more luminous ULIRGs, rather than increasing the AGN dominance with increasing total luminosity.

(iii) We derive a mean starburst age range in ULIRGs of 1.0×10^7–4.0×10^7 yr. Together with previous estimates for the lifetime of a ULIRG and an AGN, we find that most ULIRGs must undergo multiple starbursts during their lifetime. When combined with recent simulations of pair and multiple galaxy mergers we infer that mergers between more than two galaxies may be common in the ULIRG population.

(iv) By comparison with previous results we find that the mid-IR $F_{7.7}/C_{7.7}$ line-continuum ratio gives no indication of the luminosity of the starburst in ULIRGs. We also find that the $F_{7.7}/C_{7.7}$ ratio gives no indication of the fractional AGN luminosity. We therefore

find that a large value of $F_{7.7}/C_{7.7}$ only indicates the presence of a moderately obscured starburst, but gives no information on the presence or properties of heavily obscured starbursts and AGN. As such, the $F_{7.7}/C_{7.7}$ ratio on its own is not a reliable diagnostic of the power source in ULIRGs.

(v) The total 1.4-GHz radio flux for the objects in our sample correlates strongly with the starburst luminosity but shows no correlation with the AGN luminosity. From this we infer that the radio–IR correlation in ULIRGs is due to star formation, in line with previous results. Furthermore, we propose that the scatter in the correlation is due to a skewed IMF of the starburst and/or a relic relativistic electron population from a previous starburst event, rather than contamination from an obscured AGN.

(vi) The rarity of luminous AGN and AGN-dominated systems argues against a simple evolutionary model for ULIRGs in which they all evolve to become optical QSOs. Furthermore, although 'warm' ULIRGs generally contain more luminous AGN than do the 'cool' ULIRGs, there is no difference in fractional AGN luminosity between the 'warm' ULIRGs and the 'cool' ULIRGs. We therefore find that ULIRGs as a class do not evolve to become QSOs, but instead follow multiple evolutionary paths in transforming merging spirals into emerging ellipticals, and that only a few ULIRGs become optical QSOs, as suggested by Farrah et al. (2001).

(vii) By comparing our local sample with a sample of HLIRGs at $z \sim 1$ we find that AGN activity is much higher in the $z \sim 1$ sample. We infer that the two samples are distinct populations and postulate that different galaxy formation processes at high z are responsible for this difference.

ACKNOWLEDGMENTS

We thank Ben Tristem for helpful discussions, and the referee for a very helpful report. The work presented has made use of the NASA/IPAC Extragalactic Data base (NED), which is operated by the Jet Propulsion Laboratory under contract with NASA, and the Digitized Sky Surveys, which were produced at the Space Telescope Science Institute under US Government grant NAG W-2166. The images of these surveys are based on photographic data obtained using the Oschin Schmidt Telescope on Palomar Mountain and the UK Schmidt Telescope. This work was in part supported by PPARC (grant number GR/K98728). DF was supported in part for this work by NASA grant NAG 5-3370 and by the Jet Propulsion Laboratory, California Institute of Technology, under contract with NASA. JA gratefully acknowledges the support from the Science and Technology Foundation (FCT, Portugal) through the fellowship BPD-5535-2001 and the research grant ESO-FNU-43805-2001.

REFERENCES

Arribas S., Colina L., Clements D., 2001, ApJ, 560, 160
Barger A.J., Cowie L.L., Sanders D.B., Fulton E., Taniguchi Y., Sato Y., Kawara K., Okuda H., 1998, Nat, 394, 248
Barnes J., 1989, Nat, 338, 132
Bekki K., 2001, ApJ, 2001 ApJ, 546, 189
Borne K.D., Bushouse H., Lucas R.A., Colina L., 2000, ApJ, 529, L77
Bruzual A.G., Charlot S., 1993, ApJ, 405, 538
Canalizo G., Stockton A., 2001, ApJ, 555, 719
Carico D.P., Sanders D.B., Soifer B.T., Elias J.H., Matthews K., Neugebauer G., 1988, AJ, 95, 356
Carilli C.L., Taylor G.B., 2000, ApJ, 532, L95
Clements D.L., Sutherland W.J., Saunders W., Efstathiou G.P., McMahon R.G., Maddox S., Lawrence A., Rowan-Robinson M., 1996, MNRAS, 279, 459
Clements D.L., McDowell J.C., Shaked S., Baker A.C., Borne K., Colina L., Lamb S.A., Mundell C., 2002, ApJ, 581, 974
Charmandaris V. et al., 2002, A&A, 391, 429
Chini R., Kreysa E., Kruegel E., Mezger P.G., 1986, A&A, 166, L8
Colina L., Lipari S., Macchetto F., 1991, ApJ, 379, 113
Condon J.J., 1992, ARA&A, 30, 575
Condon J.J., Huang Z.-P., Yin Q.F., Thuan T.X., 1991, ApJ, 378, 65
Cram L.E., North A., Savage A., 1992, MNRAS, 257, 602
Cui J., Xia X.-Y., Deng Z.-G., Mao S., Zou Z.-L., 2001, AJ, 122, 63
Cutri R.M., Rieke G.H., Lebofsky M.J., 1984, ApJ, 287, 566
Dale D.A. et al., 2000, AJ, 120, 583
Devereux N.A., Young J.S., 1990, ApJ, 359, 42
Diamond P.J., Goss W.M., Romney J.D., Booth R.S., Kalberla P.M.W., Mebold U., 1989, ApJ, 347, 302
Dudley C.C., 1999, MNRAS, 307, 553
Dunne L., Eales S.A., 2001, MNRAS, 327, 697
Dunne L., Eales S., Edmunds M., Ivison R., Alexander P., Clements D.L., 2000, MNRAS, 315, 115
Eales S., Lilly S., Webb T., Dunne L., Gear W., Clements D., Yun M., 2000, AJ, 120, 2244
Efstathiou A., Rowan-Robinson M., 1995, MNRAS, 273, 649
Efstathiou A., Rowan-Robinson M., Siebenmorgen R., 2000, MNRAS, 313, 734
Farrah D. et al., 2001, MNRAS, 326, 1333
Farrah D., Verma A., Oliver S., Rowan-Robinson M., McMahon R., 2002a, MNRAS, 329, 605
Farrah D., Serjeant S., Efstathiou A., Rowan-Robinson M., Verma A., 2002b, MNRAS, 335, 1163
Fischer J. et al., 1999, Ap&SS, 266, 91
Fox M.J. et al., 2002, MNRAS, 331, 839
Genzel R. et al., 1998, ApJ, 498, 579
Genzel R., Tacconi L.J., Rigopoulou D., Lutz D., Tecza M., 2001, ApJ, 563, 527
Gonçalves A.C., Véron-Cetty M.-P., Véron P., 1999, A&AS, 135, 437
Gu M., Cao X., Jiang D.R., 2001, MNRAS, 327, 1111
Haas M., Klaas U., Müller S.A.H., Chini R., Coulson I., 2001, A&A, 367, L9
Harwit M., Pacini F., 1975, ApJ, 200, L127
Heisler C.A., Vader J.P., 1994, AJ, 107, 35
Helou G., Soifer B.T., Rowan-Robinson M., 1985, ApJ, 298, L7
Hildebrand R.H., 1983, QJRAS, 24, 267
Hughes D.H. et al., 1998, Nat, 394, 241
Imanishi M., Dudley C.C., Maloney P.R., 2001, ApJ, 558, L93
Iwasawa K., 1999, MNRAS, 302, 96
Joseph R.D., Wright G.S., 1985, MNRAS, 214, 87
Klaas U., Haas M., Heinrichsen I., Schulz B., 1997, A&A, 325, L21
Klaas U. et al., 2001, A&A, 379, 823
Leech K.J., Rowan-Robinson M., Lawrence A., Hughes J.D., 1994, MNRAS, 267, 253
Levenson N.A., Weaver K.A., Heckman T.M., 2001, ApJS, 133, 269
Lilly S.J., Eales S.A., Gear W.K.P., Hammer F., Le Fevre O., Crampton D., Bond J.R., Dunne L., 1999, ApJ, 518, 641
Lonsdale Carol J., Lonsdale Colin J., Smith H.E., Diamond P., 2003, ApJ, accepted (astro-ph/0304335)
Lutz D., Veilleux S., Genzel R., 1999, ApJ, 517, L13
Madau P., Ferguson H.C., Dickinson M.E., Giavalisco M., Steidel C.C., Fruchter A., 1996, MNRAS, 283, 1388
Maiolino R., Ruiz M., Rieke G.H., Keller L.D., 1995, ApJ, 446, 561
Majewski S.R., Hereld M., Koo D.C., Illingworth G.D., Heckman T.M., 1993, ApJ, 402, 125
McLure R.J., Dunlop J.S., 2001, MNRAS, 327, 199
Melnick J., Mirabel I.F., 1990, A&A, 231, L19
Mihos J.C., Hernquist L., 1994, ApJ, 431, L9
Mihos J.C., Hernquist L., 1996, ApJ, 464, 641
Miles J.W., Houck J.R., Hayward T.L., Ashby M.L.N., 1996, ApJ, 465, 191

Mirabel I.F., Lutz D., Maza J., 1991, A&A, 243, 367
Murphy T.W., Soifer B.T., Matthews K., Armus L., 2001, ApJ, 559, 201
Pappa A., Georgantopoulos I., Stewart G.C., 2000, MNRAS, 314, 589
Rees M.J., 1984, ARA&A, 22, 471
Rieke G.H., 1976, ApJ, 210, L5
Rieke G.H., 1988, ApJ, 331, L5
Rigopoulou D, Lawrence A., Rowan-Robinson M., 1996, MNRAS, 278, 1049
Rigopoulou D., Spoon H.W.W., Genzel R., Lutz D., Moorwood A.F.M., Tran Q.D., 1999, AJ, 118, 2625
Risaliti G., Gilli R., Maiolino R., Salvati M., 2000, A&A, 357, 13
Rowan-Robinson M., Crawford J., 1989, MNRAS, 238, 523
Rowan-Robinson M., 1992, MNRAS, 258, 787
Rowan-Robinson M., 1995, MNRAS, 272, 737
Rowan-Robinson M. et al., 1997, MNRAS, 289, 490
Rowan-Robinson M., 2000, MNRAS, 316, 885
Roy A.L., Norris R.P., Kesteven M.J., Troup E.R., Reynolds J.E., 1998, MNRAS, 301, 1019
Sanders D.B., Mirabel I.F., 1996, ARA&A, 34, 749
Sanders D.B., Soifer B.T., Elias J.H., Madore B.F., Matthews K., Neugebauer G., Scoville N.Z., 1988, ApJ, 325, 74
Sanders D.B., Scoville N.Z., Soifer B.T., 1991, ApJ, 370, 158
Scott S.E. et al., 2002, MNRAS, 331, 817
Scoville N.Z. et al., 2000, AJ, 119, 991
Siebenmorgen R., Kruegel E., 1992, A&A, 259, 614
Smith C.H., Aitken D.K., Roche P.F., 1989, MNRAS, 241, 425
Smith H.E., Lonsdale C.J., Lonsdale C.J., Diamond P.J., 1998, ApJ, 493, L17
Soifer B.T. et al., 1984, ApJ, 283, L1
Sopp H.M., Alexander P., 1991, MNRAS, 251, 14
Spinoglio L., Malkan M.A., Rush B., Carrasco L., Recillas-Cruz E., 1995, ApJ, 453, 616
Sturm E. et al., 1996, A&A, 315, L133
Tacconi L.J., Genzel R., Lutz D., Rigopoulou D., Baker A.J., Iserlohe C., Tecza M., 2002, ApJ, 580, 73
Taniguchi Y., Shioya Y., 1998, ApJ, 501, L167
Taniguchi Y., Ikeuchi S., Shioya Y., 1999, ApJ, 514, L9
Tran Q.D. et al., 2001, ApJ, 552, 527
Thornley M.D., Schreiber N.M.F., Lutz D., Genzel R., Spoon H.W.W., Kunze D., Sternberg A., 2000, ApJ, 539, 641
Veilleux S., Kim D.-C., Sanders D.B., Mazzarella J.M., Soifer B.T., 1995, ApJS, 98, 171
Veilleux S., Sanders D.B., Kim D.-C., 1999, ApJ, 522, 139
Veilleux S., Kim D.-C., Sanders D.B., 2002, ApJS, 143, 315
Wiklind T., Henkel C., 1995, A&A, 297, L71
Young S., Hough J.H., Efstathiou A., Wills B.J., Bailey J.A., Ward M.J., Axon D.J., 1996, MNRAS, 281, 1206
Zink E.C., Lester D.F., Doppmann G., Harvey P.M., 2000, ApJS, 131, 413

This paper has been typeset from a TEX/LATEX file prepared by the author.